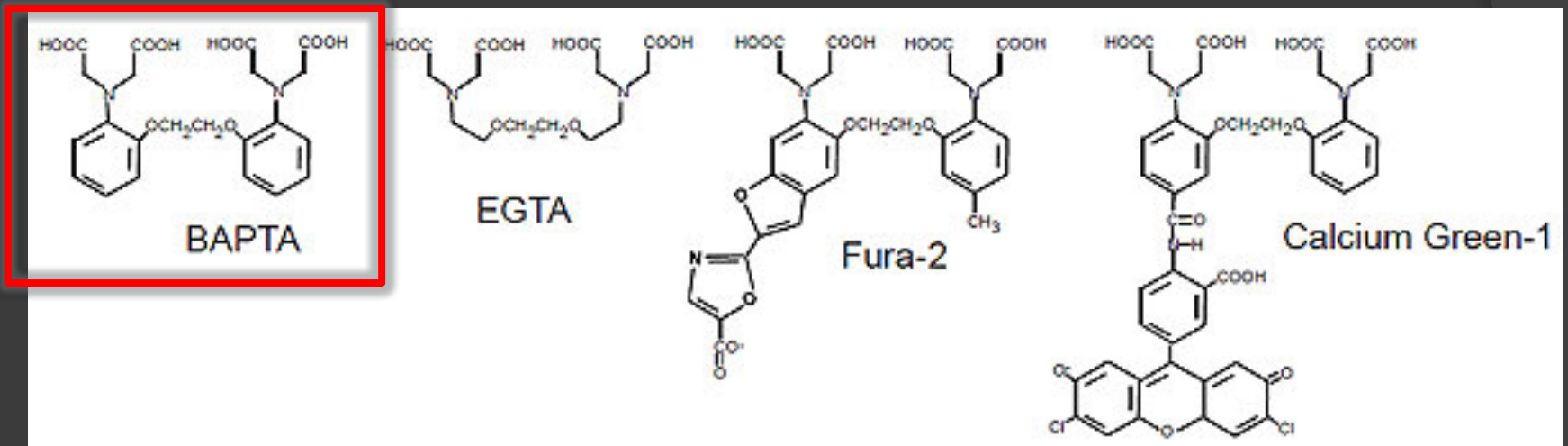


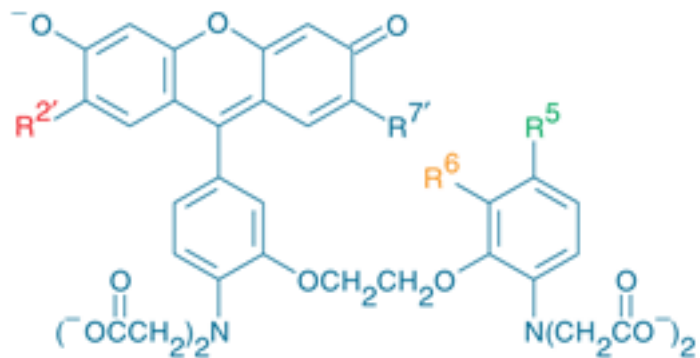
# FUNCTIONAL ANALYSES OF MEMBRANE ION CHANNELS: Ca<sup>2+</sup> signals by means of fluorescent dyes

# Synthetic Fluorescent Ca<sup>2+</sup> probes

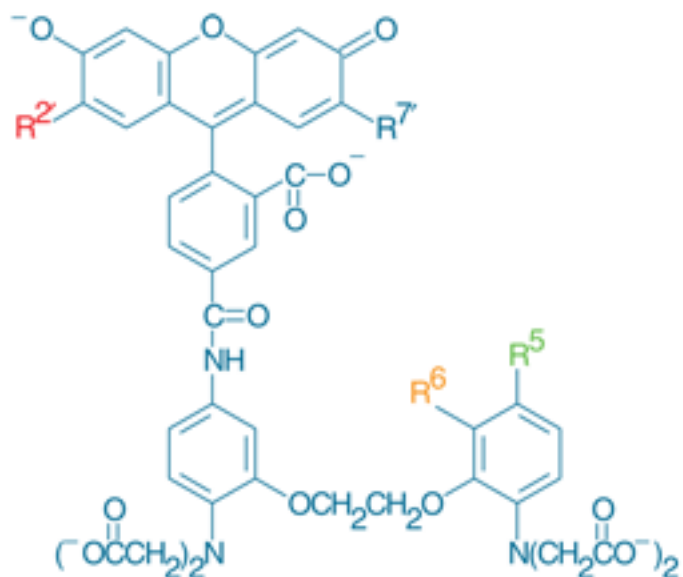
- These molecular probes specifically bind Ca<sup>2+</sup>, which causes a change in either the *intensity* or *wavelength of emission* of the probe.
- Changes in concentration of the ion can therefore be monitored.
- There are indicators for most ions, but Ca<sup>2+</sup> and pH are most commonly used.

- From the chemical point of view, most of the probes are derivatives of the  $\text{Ca}^{2+}$  chelators EGTA, and BAPTA





| Indicator | $K_d(\text{Ca}^{2+})$ | $R^{2'}$ | $R^{7'}$ | $R^5$         | $R^6$ |
|-----------|-----------------------|----------|----------|---------------|-------|
| Fluo-3    | 0.39 $\mu\text{M}$    | Cl       | Cl       | $\text{CH}_3$ | H     |
| Fluo-4    | 0.35 $\mu\text{M}$    | F        | F        | $\text{CH}_3$ | H     |
| Fluo-5F   | 2.3 $\mu\text{M}$     | F        | F        | F             | H     |
| Fluo-5N   | 90 $\mu\text{M}$      | F        | F        | $\text{NO}_2$ | H     |
| Fluo-4FF  | 9.7 $\mu\text{M}$     | F        | F        | F             | F     |

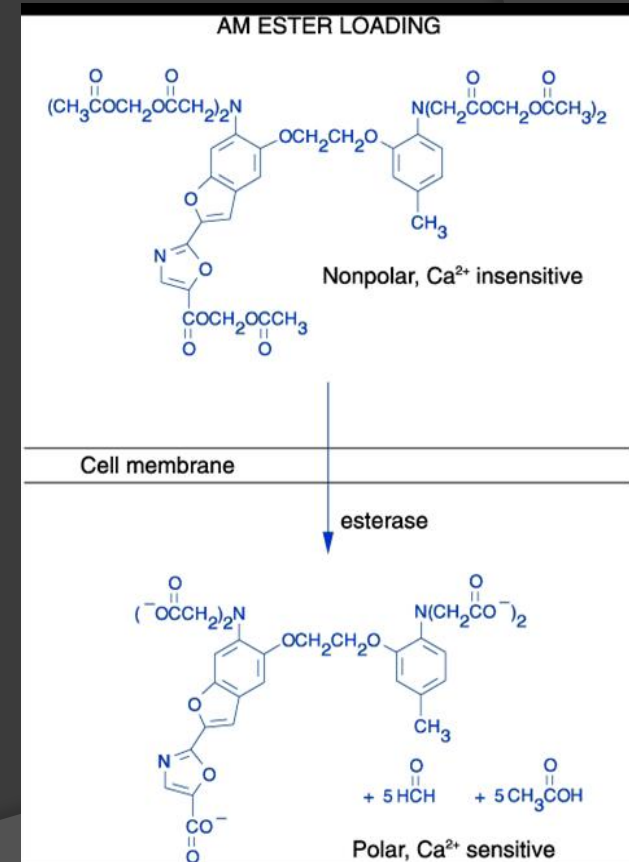


| Indicator                 | $K_d(\text{Ca}^{2+})$ | $R^{2'}$ | $R^{7'}$ | $R^5$         | $R^6$ |
|---------------------------|-----------------------|----------|----------|---------------|-------|
| Calcium Green-1           | 0.19 $\mu\text{M}$    | Cl       | Cl       | H             | H     |
| Calcium Green-5N          | 14 $\mu\text{M}$      | Cl       | Cl       | $\text{NO}_2$ | H     |
| Oregon Green 488 BAPTA-1  | 0.17 $\mu\text{M}$    | F        | F        | H             | H     |
| Oregon Green 488 BAPTA-6F | 3 $\mu\text{M}$       | F        | F        | H             | F     |
| Oregon Green 488 BAPTA-5N | 20 $\mu\text{M}$      | F        | F        | $\text{NO}_2$ | H     |

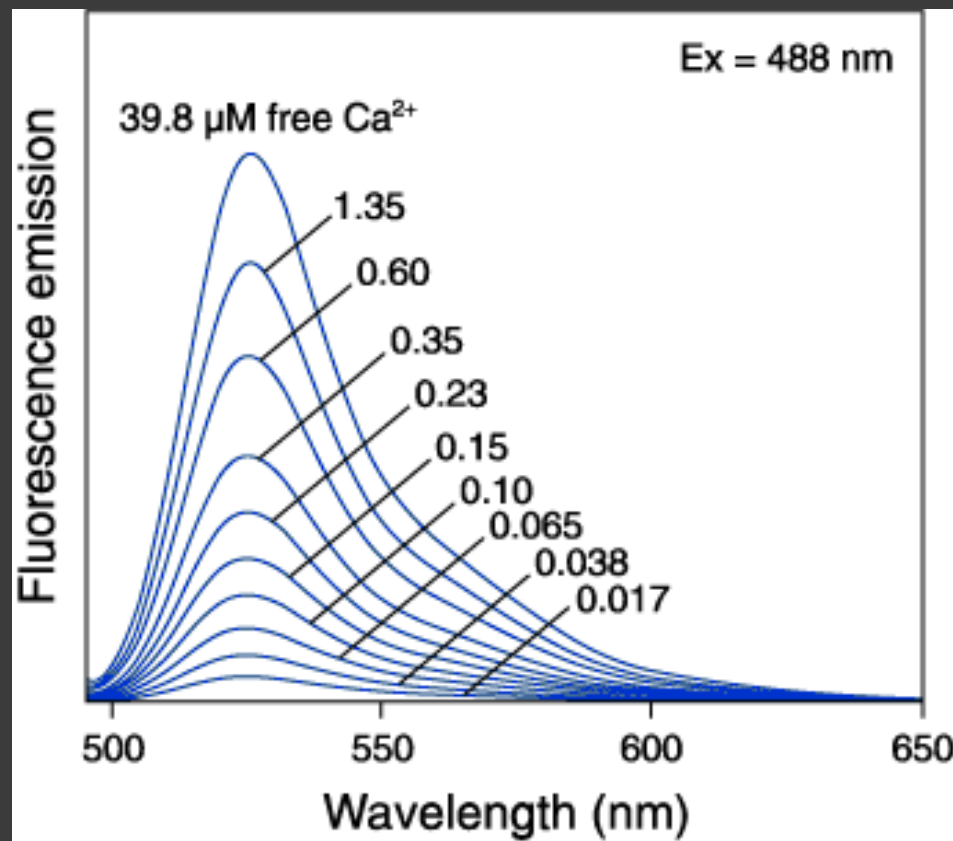


# probe incorporation (loading) into the cell

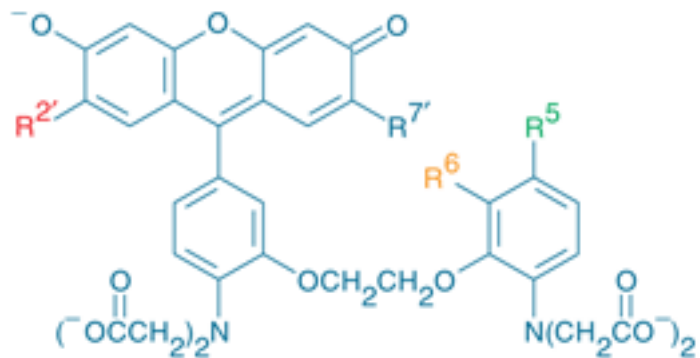
Salt or dextran forms must be microinjected; ester derivatives can be taken up by cells where they are converted to impermeant form. The carboxylate groups of indicators for  $\text{Ca}^{2+}$  and other cations and the phenolic hydroxyl groups of pH indicators are **derivatized as acetoxymethyl or acetate esters**, respectively, **rendering the indicator permeant to membranes and insensitive to ions**. Once inside the cell, these derivatized indicators are **hydrolyzed by ubiquitous intracellular esterases**, releasing the **ion-sensitive polyanionic indicator**.



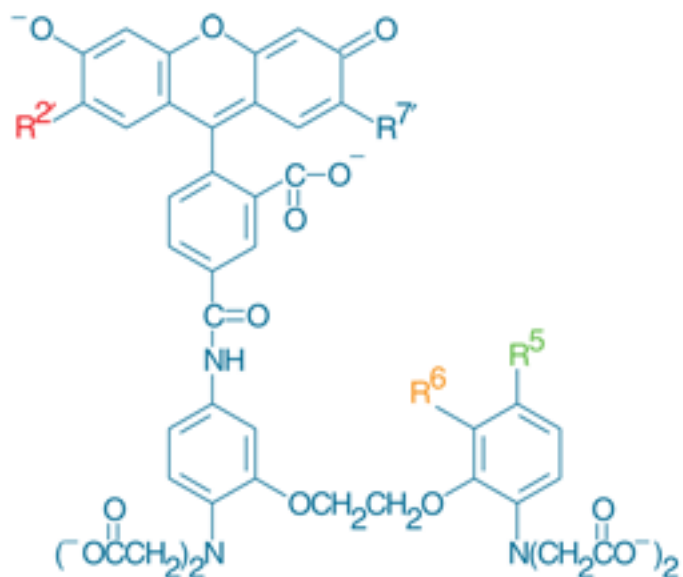
# Ca<sup>2+</sup> Indicators: Fluo-3 has single Ex and Em wavelengths



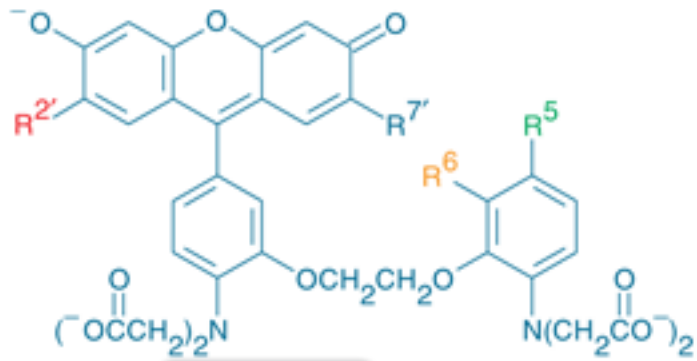
- A visible light excitable dye (488 nm), so Argon laser can be used.
- Emission at 525 nm.
- OK for qualitative detection but not quantitative.



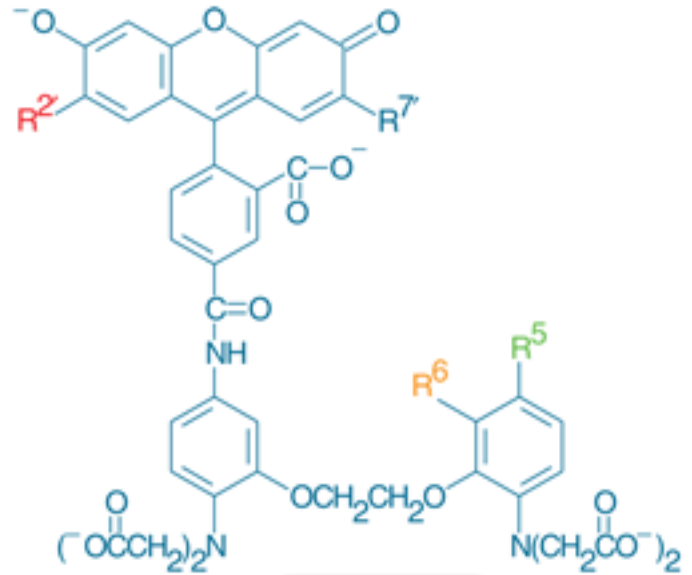
| Indicator | $K_d(\text{Ca}^{2+})$ | $R^{2'}$ | $R^{7'}$ | $R^5$         | $R^6$ |
|-----------|-----------------------|----------|----------|---------------|-------|
| Fluo-3    | 0.39 $\mu\text{M}$    | Cl       | Cl       | $\text{CH}_3$ | H     |
| Fluo-4    | 0.35 $\mu\text{M}$    | F        | F        | $\text{CH}_3$ | H     |
| Fluo-5F   | 2.3 $\mu\text{M}$     | F        | F        | F             | H     |
| Fluo-5N   | 90 $\mu\text{M}$      | F        | F        | $\text{NO}_2$ | H     |
| Fluo-4FF  | 9.7 $\mu\text{M}$     | F        | F        | F             | F     |



| Indicator                 | $K_d(\text{Ca}^{2+})$ | $R^{2'}$ | $R^{7'}$ | $R^5$         | $R^6$ |
|---------------------------|-----------------------|----------|----------|---------------|-------|
| Calcium Green-1           | 0.19 $\mu\text{M}$    | Cl       | Cl       | H             | H     |
| Calcium Green-5N          | 14 $\mu\text{M}$      | Cl       | Cl       | $\text{NO}_2$ | H     |
| Oregon Green 488 BAPTA-1  | 0.17 $\mu\text{M}$    | F        | F        | H             | H     |
| Oregon Green 488 BAPTA-6F | 3 $\mu\text{M}$       | F        | F        | H             | F     |
| Oregon Green 488 BAPTA-5N | 20 $\mu\text{M}$      | F        | F        | $\text{NO}_2$ | H     |



| Indicator | $K_d(\text{Ca}^{2+})$ | $R^{2'}$ | $R^{7'}$ | $R^5$         | $R^6$ |
|-----------|-----------------------|----------|----------|---------------|-------|
| Fluo-3    | 0.39 $\mu\text{M}$    | Cl       | Cl       | $\text{CH}_3$ | H     |
| Fluo-4    | 0.35 $\mu\text{M}$    | F        | F        | $\text{CH}_3$ | H     |
| Fluo-5F   | 2.3 $\mu\text{M}$     | F        | F        | F             | H     |
| Fluo-5N   | 90 $\mu\text{M}$      | F        | F        | $\text{NO}_2$ | H     |
| Fluo-4FF  | 9.7 $\mu\text{M}$     | F        | F        | F             | F     |

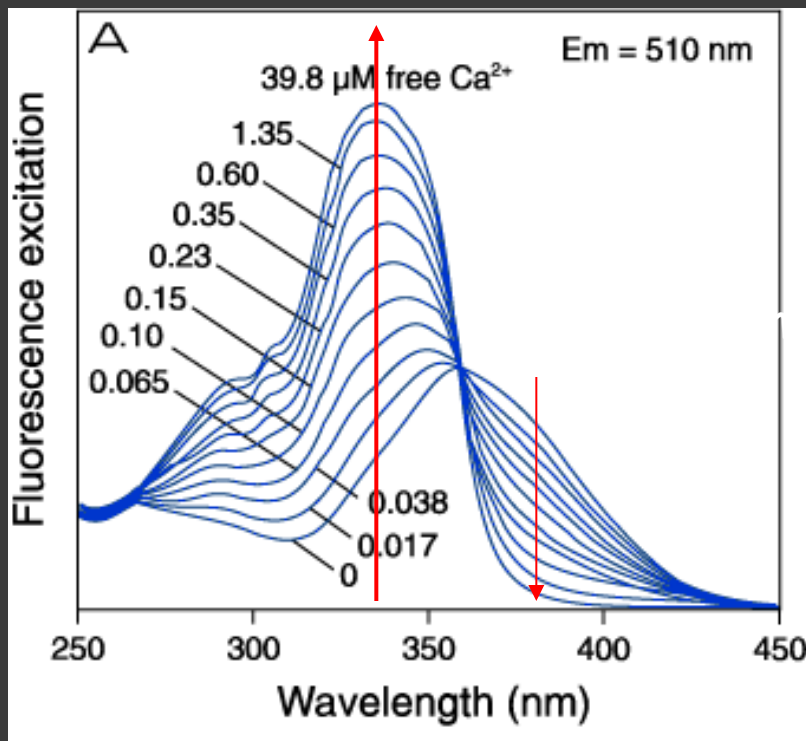


| Indicator                 | $K_d(\text{Ca}^{2+})$ | $R^{2'}$ | $R^{7'}$ | $R^5$         | $R^6$ |
|---------------------------|-----------------------|----------|----------|---------------|-------|
| Calcium Green-1           | 0.19 $\mu\text{M}$    | Cl       | Cl       | H             | H     |
| Calcium Green-5N          | 14 $\mu\text{M}$      | Cl       | Cl       | $\text{NO}_2$ | H     |
| Oregon Green 488 BAPTA-1  | 0.17 $\mu\text{M}$    | F        | F        | H             | H     |
| Oregon Green 488 BAPTA-6F | 3 $\mu\text{M}$       | F        | F        | H             | F     |
| Oregon Green 488 BAPTA-5N | 20 $\mu\text{M}$      | F        | F        | $\text{NO}_2$ | H     |

The  $K_d$  has molar units and corresponds to the concentration of  $\text{Ca}^{2+}$  at which half the indicator molecules are bound with  $\text{Ca}^{2+}$  at equilibrium. When possible, indicators should be utilized to measure  $\text{Ca}^{2+}$  concentrations between 0.1 and 10 times their  $K_d$ . This is the range over which  $\text{Ca}^{2+}$  dependent changes in fluorescence are the largest.

# UV Ca<sup>2+</sup> Indicators: Fura-2 is a fixed emission ratiometric dye

Ex at 340 nm and 380 nm

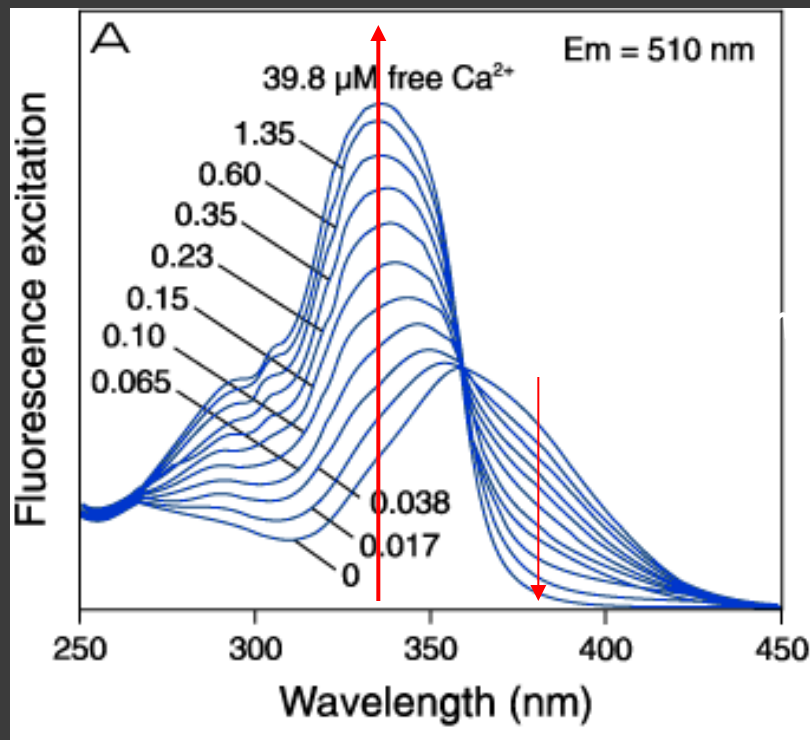


Fura-2

Fura-2 has very limited sensitivity to Ca<sup>2+</sup> concentrations above 1  $\mu\text{M}$ . Furthermore, rapid Ca<sup>2+</sup> transients monitored by fura-2 photometry are often damped due to the slow rate of Ca<sup>2+</sup> dissociation from the indicator. For these reasons, Molecular Probes offers several fura-2 derivatives with lower Ca<sup>2+</sup> binding affinity (i.e., higher K<sub>d</sub> (Ca<sup>2+</sup>); Table 1).

# UV Ca<sup>2+</sup> Indicators: Fura-2 is a fixed emission ratiometric dye

Ex at 340 nm and 380 nm



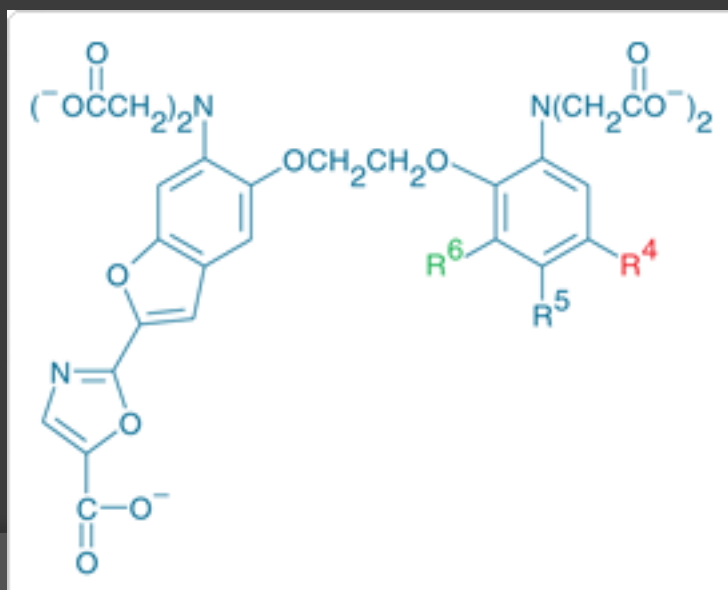
Fura-2

- excitation at 340 and 380 nm. emission at 510 nm
- Ratioing considerably reduces the effects of uneven dye loading, leakage of dye, and photobleaching, as well as problems associated with measuring Ca<sup>2+</sup> in cells of unequal thickness.
- In addition, fura-2 and indo-1 are bright enough to permit measurements at intracellular concentrations of dye unlikely to cause significant Ca<sup>2+</sup> buffering or damping of Ca<sup>2+</sup> transients.

**Table 1.** Spectroscopic properties and Ca<sup>2+</sup> dissociation constants for fura-2, indo-1, and their derivatives.

| Indicator  | Catalog Number  |                                  | Zero Calcium             |   |                       | High Calcium             |   |                       | K <sub>d</sub> (Ca <sup>2+</sup> )<br>(μM) |
|------------|-----------------|----------------------------------|--------------------------|---|-----------------------|--------------------------|---|-----------------------|--|
|            | Salt            | AM Ester                         | λ <sub>A</sub> †<br>(nm) | ε <sub>max</sub> ‡<br>(cm <sup>-1</sup> M <sup>-1</sup> ) | λ <sub>F</sub> § (nm) | λ <sub>A</sub> †<br>(nm) | ε <sub>max</sub> ‡<br>(cm <sup>-1</sup> M <sup>-1</sup> ) | λ <sub>F</sub> § (nm) |  |
| fura-2     | F1200,<br>F6799 | F1201, F1221, F1225,<br>F14185 * | 363                      | 28,000  | 512 **                | 335                      | 34,000  | 505 ††                | 0.14                                       |
| bis-fura-2 | B6810           |                                  | 366                      | 56,000  | 511                   | 338                      | 68,000  | 504                   | 0.37                                       |
| fura-5F    | F14176          | F14177                           | 363                      | 26,000  | 512                   | 336                      | 29,000  | 506                   | 0.40                                       |
| fura-4F    | F14174          | F14175                           | 366                      | 21,000  | 511                   | 336                      | 23,000  | 505                   | 0.77                                       |
| fura-6F    | F14178          | F14179                           | 364                      | 25,000  | 512                   | 336                      | 28,000  | 505                   | 5.30                                       |
| fura-FF    | F14180          | F14181                           | 364                      | 25,000  | 510                   | 335                      | 28,000  | 506                   | 5.50                                       |
| indo-1     | I1202           | I1203, I1223, I1226              | 346                      | 33,000  | 475 **                | 330                      | 33,000  | 401 ††                | 0.23                                       |
| indo-5F    | I23912          | I23913                           | 344                      | 31,000  | 471                   | 329                      | 31,000  | 398                   | 0.47                                       |

\* High-purity FluoroPure™ grade; † absorption maximum; ‡ molar extinction coefficient; § fluorescence emission maximum; \*\* fluorescence quantum yield 0.23 for fura-2, 0.38 for indo-1. †† Fluorescence quantum yield 0.49 for fura-2, 0.56 for indo-1. Spectroscopic data and K<sub>d</sub> (dissociation constant) values measured in 100 mM KCl, 10 mM MOPS, pH 7.20, 0–10 mM CaEGTA at 22°C.



# Measurements and Calibration for Fura Indicators

- In contrast to single-wavelength indicators such as fluo-3, the absorption (or fluorescence excitation) maximum of fura indicators shifts from 363 nm for the  $\text{Ca}^{2+}$ -free chelator to about 335 nm for the  $\text{Ca}^{2+}$ -bound. The wavelength of maximum fluorescence emission is relatively independent of  $\text{Ca}^{2+}$  concentration (Table 1). The largest dynamic range for  $\text{Ca}^{2+}$ -dependent fluorescence signals is obtained by using excitation at 340 nm and 380 nm and ratioing the fluorescence intensities detected at  $\sim 510$  nm. From this ratio, the level of intracellular  $\text{Ca}^{2+}$  can be estimated, using dissociation constants ( $K_d$ ) that are derived from calibration curves.



# Measurements and Calibration for Fura Indicators

- By using the *ratio* of fluorescence intensities produced by excitation at two wavelengths factors such as uneven dye distribution and photobleaching are minimized because they should affect both measurements to the same extent.

# Measurements and Calibration for Fura Indicators

Once the indicator has been calibrated with solutions of known  $\text{Ca}^{2+}$  concentrations, the following equation can be used to relate the intensity ratios to  $\text{Ca}^{2+}$  levels:

$$[\text{Ca}^{2+}] = K_d Q \frac{(R - R_{\min})}{(R_{\max} - R)}$$

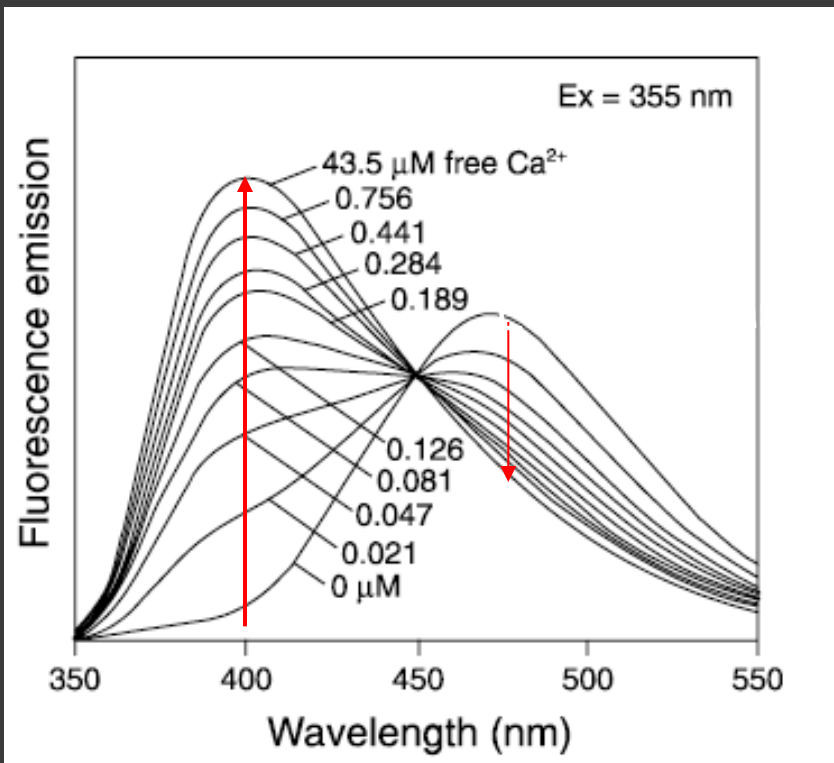
**R** represents the **fluorescence intensity ratio**  $F_{\lambda 1}/F_{\lambda 2}$ , in which  $\lambda 1$  (~340 nm) and  $\lambda 2$  (~380 nm) are the fluorescence detection wavelengths for the ion-bound and ion-free indicator, respectively. Ratios corresponding to the titration end points are denoted by the subscripts indicating the minimum and maximum  $\text{Ca}^{2+}$  concentration.

**Q** is the **ratio of  $F_{\min}$  to  $F_{\max}$  at  $\lambda 2$**  (~380 nm).

**K<sub>d</sub>** is the  **$\text{Ca}^{2+}$  dissociation constant of the indicator**. Calibrating fura indicators requires making measurements for the completely ion-free and ion-saturated indicator (to determine the values for  $F_{\min}$ ,  $F_{\max}$ ,  $R_{\min}$ , and  $R_{\max}$ ) and for the indicator in the presence of known  $\text{Ca}^{2+}$  concentrations (to determine  $K_d$ ).

# UV $\text{Ca}^{2+}$ Indicators: **Indo-1** is a fixed excitation ratiometric dye

Em at 400 nm and 480 nm



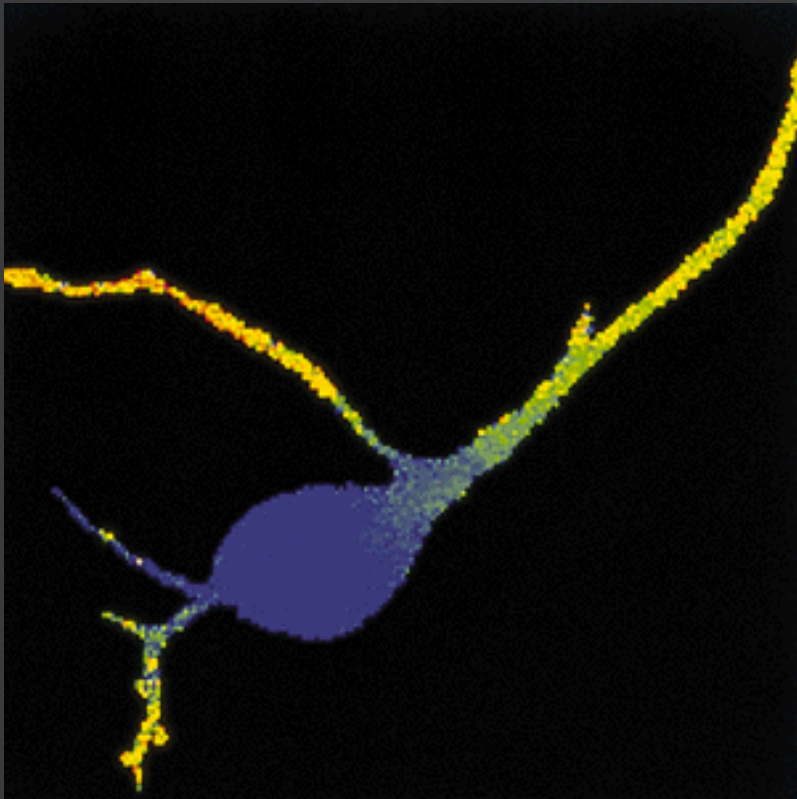
**Indo-1**

Indo-1 shares most of the advantages of fura indicators except that it is somewhat more light-sensitive. In contrast to fura indicators, which exhibit large changes in absorption on  $\text{Ca}^{2+}$  binding, the emission of indo-1 shifts from about 475 nm without  $\text{Ca}^{2+}$  to about 400 nm with  $\text{Ca}^{2+}$  when excited at about 350 nm.

Equation 1 above may be used for the calibration of indo-1. For this indicator, the value of  $\lambda_1$  is 405 nm while  $\lambda_2$  is 485 nm.

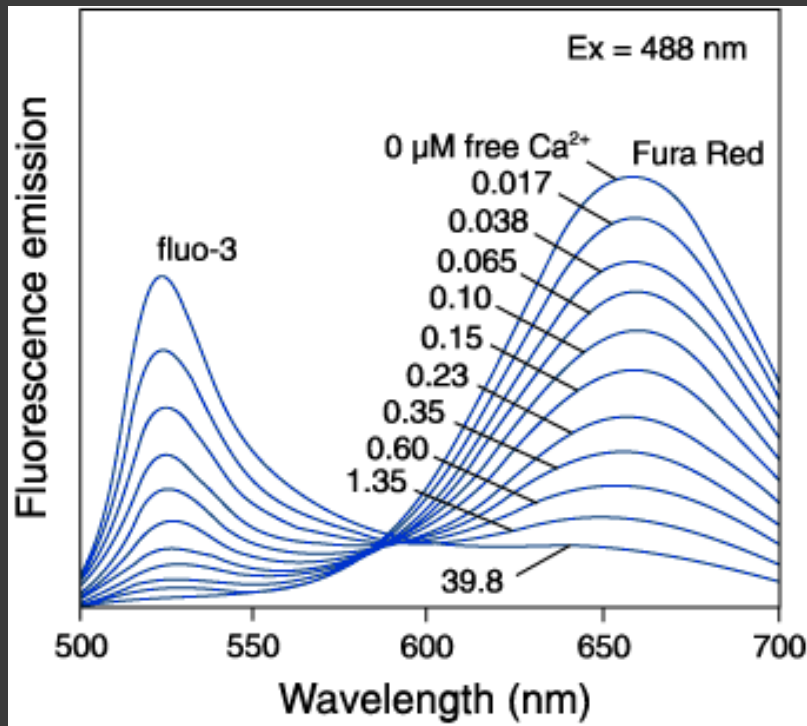
Indo-1 is especially useful for flow cytometry where it is easier to change the emission filters with a single excitation source (often the ultraviolet lines of the argon-ion laser in flow cytometers), and is particularly suited for multicolor fluorescence applications.

# Free $\text{Ca}^{2+}$ Concentration in a Purkinje Neuron from Embryonic Mouse Cerebellum



- Neurons were loaded with fura-2.
- Neurons were stimulated with glutamate receptor agonist.
- The composite image represents the ratio of images obtained with excitation at 340 nm and 380 nm.

# Dual Blue Ca<sup>2+</sup> Indicators: Fluo-3 and Fura Red



- Use of two dyes solves the problem, e.g. Fluo-3 (increase at 525 with increasing [Ca<sup>2+</sup>]) and Fura Red (decrease at 650 upon increasing [Ca<sup>2+</sup>]).
- Both excited by 488 nm.
- [Ca<sup>2+</sup>] ~ Em of Fluo-3 / Em of Fura Red, independent of [dye].

# Genetically encoded Ca<sup>2+</sup> indicators (GECI)

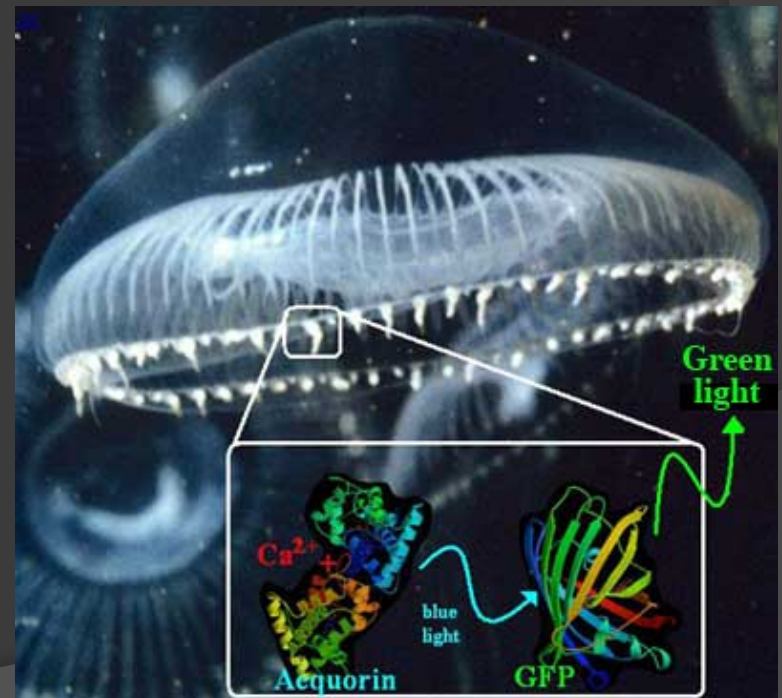
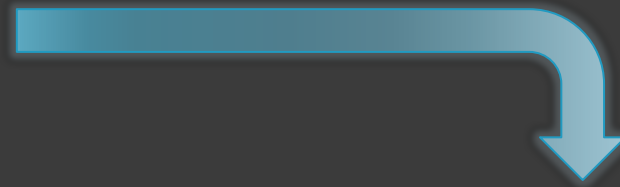
Intracellular Ca<sup>2+</sup> detection.

| Probe                | Origin              | Detection technique                 | Ref. |
|----------------------|---------------------|-------------------------------------|------|
| Aequorin             | Genetically encoded | Luminometry                         | 15   |
| Berovin              | Genetically encoded | Luminometry                         | 22   |
| Obelin               | Genetically encoded | Luminometry                         | 23   |
| Cameleon             | Genetically encoded | FRET microscopy                     | 24   |
| Troponin C biosensor | Genetically encoded | FRET microscopy                     | 25   |
| Camgaroo             | Genetically encoded | Fluorescence microscopy             | 26   |
| Ratiometric Pericam  | Genetically encoded | Ratiometric fluorescence microscopy | 27   |
| GEM-GECO1            | Genetically encoded | Ratiometric fluorescence microscopy | 28   |
| Calcium Green-1      | Synthetic           | Fluorescence microscopy             | 29   |
| Fluo-3, Fluo-4       | Synthetic           | Fluorescence microscopy             | 29   |
| Fura-2, Indo-1       | Synthetic           | Ratiometric fluorescence microscopy | 30   |

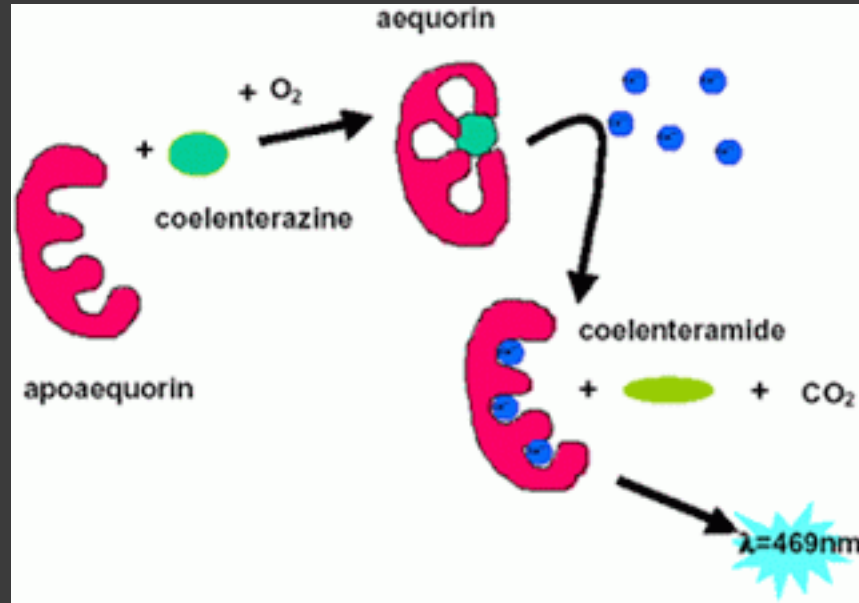
# Genetically encoded Ca<sup>2+</sup> indicators (GECI)

Intracellular Ca<sup>2+</sup> detection.

| Probe                | Origin              | Detection technique                 | Ref. |
|----------------------|---------------------|-------------------------------------|------|
| Aequorin             | Genetically encoded | Luminometry                         | 15   |
| Berovin              | Genetically encoded | Luminometry                         | 22   |
| Obelin               | Genetically encoded | Luminometry                         | 23   |
| Cameleon             | Genetically encoded | FRET microscopy                     | 24   |
| Troponin C biosensor | Genetically encoded | FRET microscopy                     | 25   |
| Camgaroo             | Genetically encoded | Fluorescence microscopy             | 26   |
| Ratiometric Pericam  | Genetically encoded | Ratiometric fluorescence microscopy | 27   |
| GEM-GECO1            | Genetically encoded | Ratiometric fluorescence microscopy | 28   |
| Calcium Green-1      | Synthetic           | Fluorescence microscopy             | 29   |
| Fluo-3, Fluo-4       | Synthetic           | Fluorescence microscopy             | 29   |
| Fura-2, Indo-1       | Synthetic           | Ratiometric fluorescence microscopy | 30   |



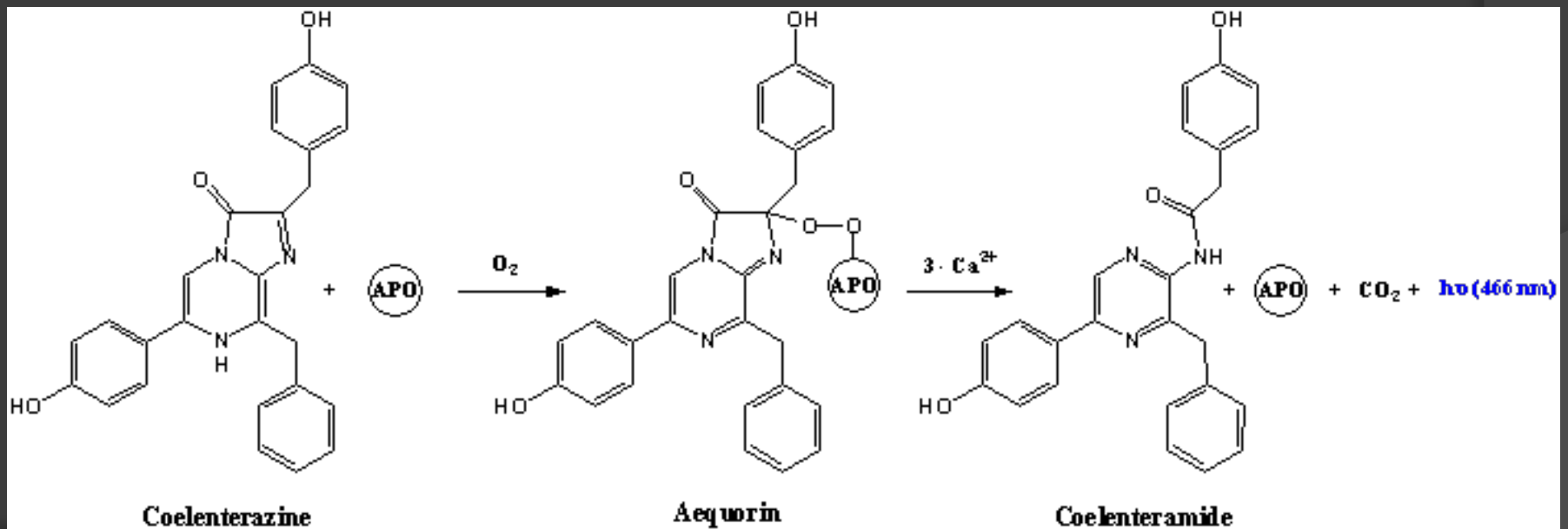
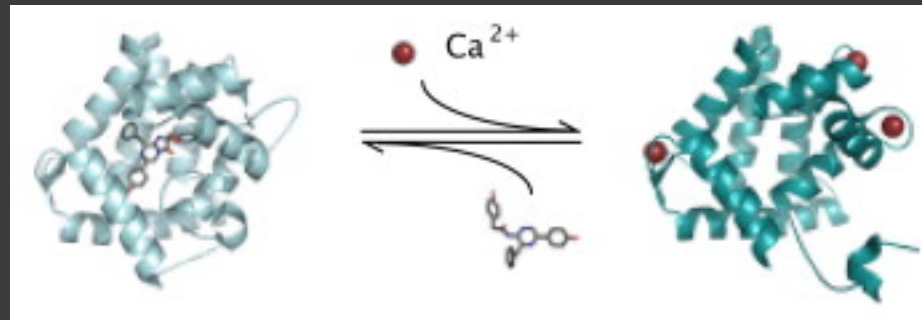
# AEQUORIN



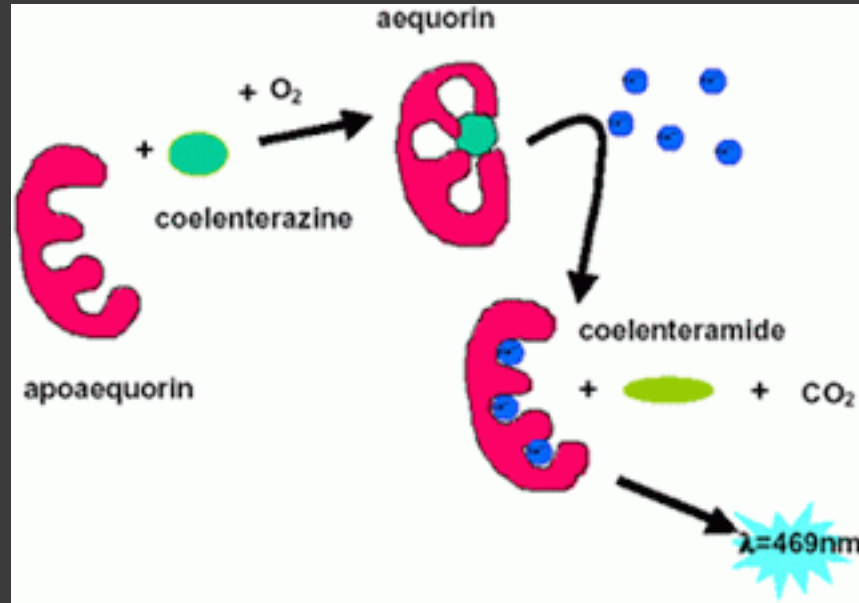
22-kDa protein has had a major role in the study of  $Ca^{2+}$  signaling. Upon binding of  $Ca^{2+}$  to three high-affinity sites, aequorin undergoes an irreversible reaction in which a photon is emitted. In its active form, the protein includes a prosthetic group (coelenterazine) that is oxidized and released in the  $Ca^{2+}$ -triggered reaction.



# AEQUORIN



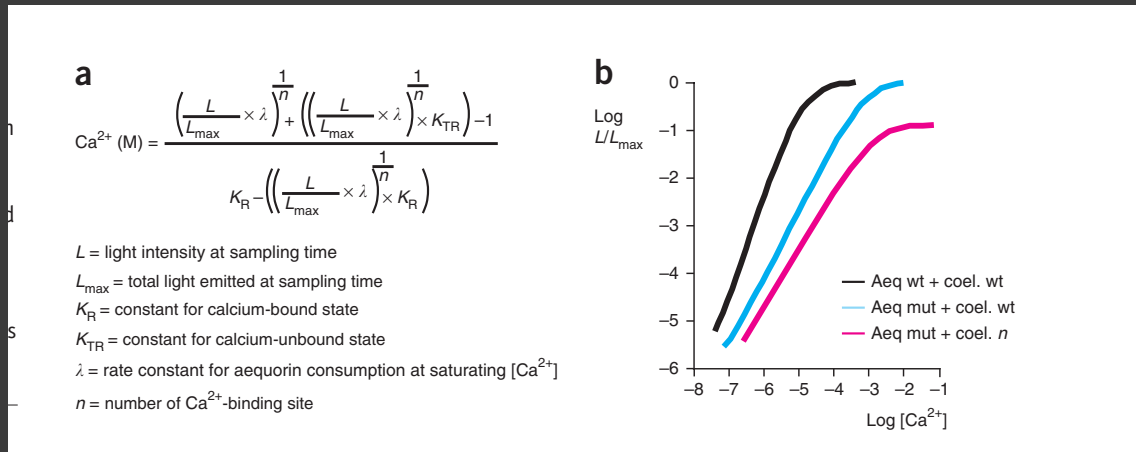
# AEQUORIN



Thus, the expression of aequorin cDNA yields the polypeptide, to which the prosthetic group must be added. Coelenterazine is highly hydrophobic and, when added to the culture medium of aequorin-expressing cells, will freely permeate through the cell membrane. Once inside the cell, coelenterazine spontaneously binds to aequorin, generating the active probe. This procedure is generally termed 'reconstitution'.

# AEQUORIN

There is a relationship between the fractional rate of consumption (i.e.,  $L/L_{\max}$ , where  $L_{\max}$  is the maximal rate of discharge at saturating  $\text{Ca}^{2+}$  concentrations) and  $[\text{Ca}^{2+}]$ .



Owing to cooperation between the three binding sites, light emission is proportional to the second to third power of  $[\text{Ca}^{2+}]$ ; this property on the one hand accounts for the **excellent signal-to-noise ratio of aequorin** and on the other hand may substantially affect the measurements.

# AEQUORIN

Given that the probe (differently from fluorescent indicators) is gradually consumed throughout the experiment, the signal tends to decrease, and the conversion into  $[Ca^{2+}]$  concentration can be obtained only at the end of the experiment, when, after cell lysis, the total aequorin content is estimated and  $L/L_{max}$  can be back calculated for each data point.

# Major advantages of using aequorin

## **Selective intracellular distribution.**

The main reason for the renewed interest in using aequorin is that, being a protein, it can be engineered to induce its specific localization to a cell region of interest. Although wild-type aequorin is exclusively cytosolic (cytAEQ), the addition of specific targeting sequences permits selective localization of the photoprotein, resulting in recombinant aequorin chimeras for different intracellular compartments: nucleus (nuAEQ), mitochondria (mtAEQ and mimsAEQ), subplasma-membrane cytosol (pmAEQ), endoplasmic/sarcoplasmic reticulum (erAEQ/srAEQ), Golgi apparatus (goAEQ), secretory vesicles (vampAEQ) and peroxisomes (peroxAEQ).

**TABLE 2** | Description of the compartment-specific aequorin chimeras available.

| Intracellular localization        | Acronym        | Targeting strategy   |
|-----------------------------------|----------------|--|
| Cytosol                           | CytAEQ         | No targeting sequence is added to aequorin; the sequence of aequorin was modified only by adding the epitope tag HA1 (ref. 15)   |
| Nucleus                           | NuAEQ          | A fragment of rat glucocorticoid receptor, lacking the hormone-binding domain and the nuclear localization signal are fused with the HA1-tagged aequorin <sup>31</sup>   |
|                                   | MtAEQwt        | Mitochondrial pre-sequence of subunit VIII of cytochrome <i>c</i> oxidase (COX) is fused to the HA1-tagged aequorin, for measurements of [Ca <sup>2+</sup> ] up to 10–15 μM (ref. 32)  |
| Mitochondrial matrix              | mtAEQmut       | The mutated version of mtAEQwt. Because of the cooperativity between the three Ca <sup>2+</sup> -binding sites of aequorin, the point mutation (Asp119Ala) <sup>13</sup> that affects the second EF-hand domain, produces a mutated aequorin, which can be used to measure [Ca <sup>2+</sup> ] in the range of 10–500 μM (ref. 33)   |
|                                   | mtAEQmut28,119 | Double-mutated form (Asp119Ala and Asn28Leu) of mtAEQwt, which can be used to measure [Ca <sup>2+</sup> ] in the millimolar range for long periods of time, without problems derived from aequorin consumption <sup>14</sup>   |
| Mitochondrial intermembrane space | MimsAEQ        | HA1-tagged aequorin is fused (sequence in frame) with glycerol phosphate dehydrogenase, an integral protein of the inner mitochondrial membrane, with a large C-terminal tail protruding on the outer side of the membrane, i.e., in the mitochondrial intermembrane space <sup>34</sup>   |
| Plasma membrane                   | pmAEQ          | The targeting of aequorin to the subplasmalemmal space was based on the construction of a fusion protein including the HA1-tagged aequorin and SNAP-25, a protein that is synthesized on free ribosomes and recruited to the inner surface of the plasma membrane after the palmitoylation of specific cysteine residues <sup>35</sup>   |
| Endoplasmic reticulum             | erAEQmut       | The encoded polypeptide includes the leader sequence (L), the VDJ and CH1 domains of an Igg2b heavy chain (HC) and the HA1-tagged aequorin at the C-terminus. In this chimera, retention in the ER depends on the presence of the CH1 domain at the N terminus of aequorin. This domain is known to interact with the luminal ER protein BiP, thus causing the retention of the Igg2b HC in the lumen. In the absence of the immunoglobulin light chain, the polypeptide is retained in this compartment <sup>36</sup> |
| Sarcoplasmic reticulum            | srAEQmut       | Calsequestrin (CSQ), a resident protein of the sarcoplasmic reticulum, is fused to HA1-tagged aequorin. This chimera is used to measure [Ca <sup>2+</sup> ] in the sarcoplasmic reticulum, the specialized muscle compartment involved in the regulation of Ca <sup>2+</sup> homeostasis <sup>37</sup>   |
| Golgi apparatus                   | goAEQmut       | Fusion of the HA1-tagged aequorin and the transmembrane portion of sialyltransferase, a resident protein of the Golgi lumen <sup>18</sup>  |
| Secretory vesicles                | vampAEQmut     | Mutated AEQ (AEQmut: Asp119Ala) is fused to the vesicle-associated membrane protein (vamp)2/synaptobrevin (a vesicle-specific SNARE with a single transmembrane-spanning region) allowing intravesicular [Ca <sup>2+</sup> ] to be monitored <sup>38</sup>   |
| Peroxisomes                       | peroxAEQ       | HA1-tagged wild-type and Asp119Ala mutant aequorins were fused with a peroxisomal targeting sequence <sup>17</sup>   |

# Major advantages of using aequorin

## Wide dynamic range.

Native aequorin and its mutants (**Table 2**), in association with different prosthetic groups, are well suited for measuring  $[Ca^{2+}]$  from as low as  $0.1 \mu M$  and up into the mM range.

Numerous chemical modifications of the prosthetic group have been made, which modify, in different ways, the Ca-triggered reaction of the photoprotein. Among these, particularly useful have been those that result in lower light emission at high  $[Ca^{2+}]$ .

In parallel, single point mutations have been inserted in aequorin cDNAs to reduce its affinity and to allow measurements at higher  $Ca^{2+}$  concentrations. Combinations of mutant aequorins and modified coelenterazine have been used to further increase the dynamic range, allowing measurements in compartments with low  $[Ca^{2+}]$  (i.e., cytoplasm or mitochondria in certain cell types), high  $[Ca^{2+}]$  (i.e., peroxisomes or mitochondria of other cell) or very high  $[Ca^{2+}]$  (i.e., Golgi or ER).

# Major advantages of using aequorin

## High signal-to-noise ratio.

Mammalian cells are not endowed with chemiluminescent proteins, and thus the background of aequorin measurement is very low. Moreover, the steep relationship between the increases in light emission and  $\text{Ca}^{2+}$  concentration accounts for the very large luminescence peaks observed upon stimulation of cells (>1,000–10,000-fold over background can be detected with cytosolic and mitochondrial aequorin, respectively). Because of the excellent signal-to-noise ratio, reliable aequorin measurements can be obtained with moderate levels of expression of the probe.



# Major advantages of using aequorin

## **Low Ca<sup>2+</sup>-buffering effect.**

Aequorin displays an extremely low buffering effect on intracellular Ca<sup>2+</sup>, negligible if compared with that of fluorescent Ca<sup>2+</sup> indicators.

Thus, although in principle, all Ca<sup>2+</sup> probes perturb Ca<sup>2+</sup> homeostasis because they bind Ca<sup>2+</sup> and thus act as Ca<sup>2+</sup> buffers, this effect is much less relevant for aequorin than for trappable fluorescent dyes.

As an example, Fura-2 measurements in the presence or absence of aequorin display the same cytoplasmic Ca<sup>2+</sup> levels; on the contrary, aequorin measurements show a strong reduction in cytoplasmic [Ca<sup>2+</sup>] if Fura-2 is added compared with vehicle.

# Major disadvantages of using aequorin

## **Low light emission by the photoprotein.**

In contrast to fluorescent dyes (where up to  $10^4$  photons can be emitted by a single molecule before photobleaching occurs), only one photon can be emitted by an aequorin molecule. This means that only a small fraction of the total aequorin pool emits its photon every second: out of the  $10^4$ – $10^5$  molecules per cell of a typical aequorin transfection, light emission will vary from 0 to 1,000 photons at most.

# Major disadvantages of using aequorin

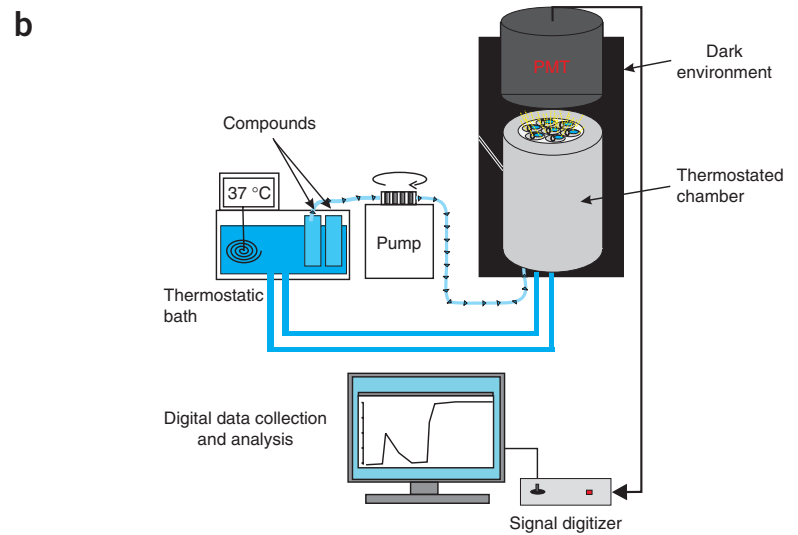
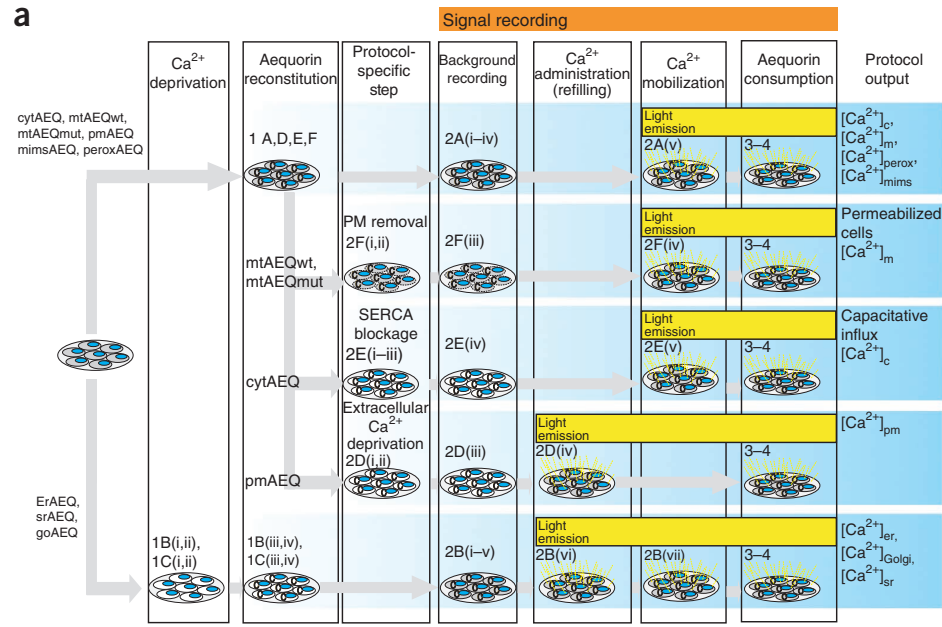
**Overestimation of the average rise in cells (or compartments) with inhomogeneous behavior.**

Because of the steep  $\text{Ca}^{2+}$  response curve of aequorin, if the probe is distributed between a high- $\text{Ca}^{2+}$  and a low- $\text{Ca}^{2+}$  domain, the former will undergo a much larger discharge. The total signal will be calibrated as 'average'  $[\text{Ca}^{2+}]$  increase, which will be severely biased by the region with high  $\text{Ca}^{2+}$ .

# Major disadvantages of using aequorin

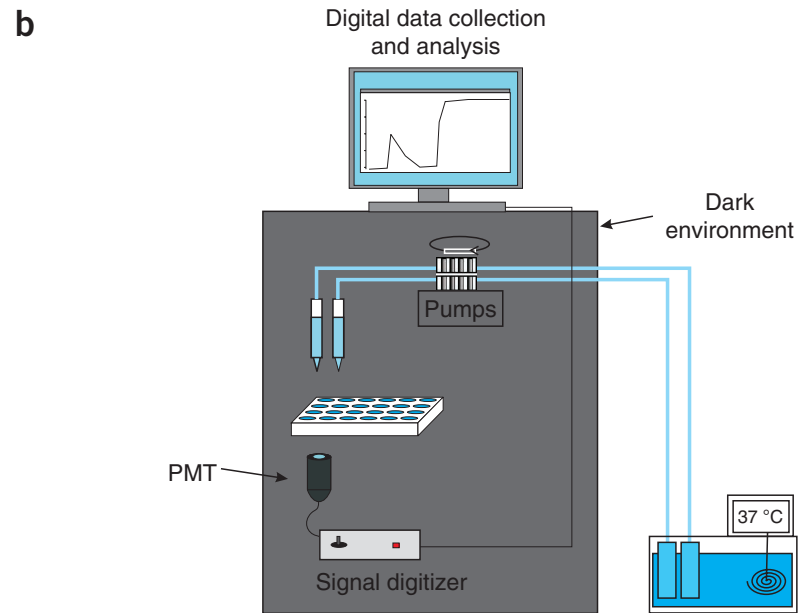
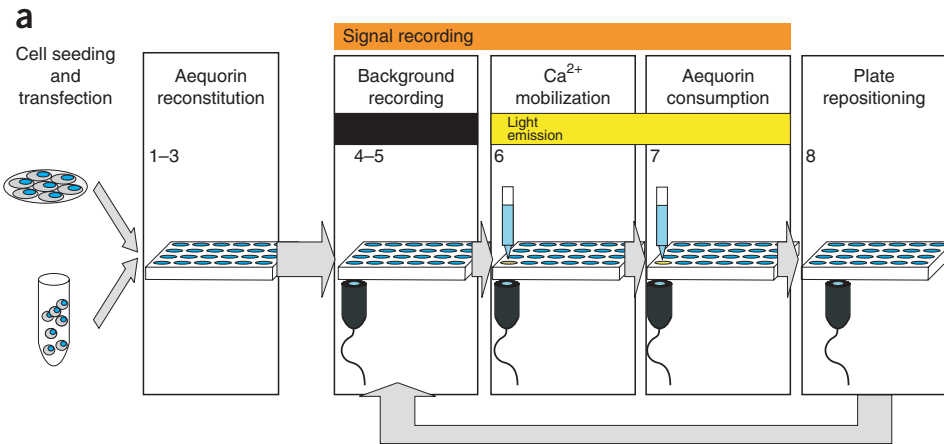
**Cells must be amenable to transfection.**

The obvious requirement of this approach is that the cell type being studied must be amenable to transfection.



Possibility to perform the experiment on automated plate reader luminometers, which allows for measurements of suspended cells, also in **high-throughput assays**.

Plate-reader luminometers display a reduced sensitivity when compared with single-tube photomultipliers, especially when 96-well plates are used



# Appropriate controls

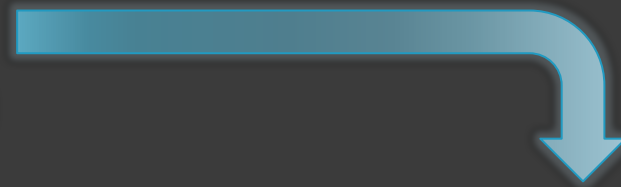
A **positive control** for probe expression is provided by cell lysis, which is done as the final phase of each procedure. Light emission induced upon cell lysis is directly proportional to the whole amount of aequorin expression.

A useful **negative control** is to perform the preferred reconstitution and recording procedure in non transfected cells

# Genetically encoded Ca<sup>2+</sup> indicators (GECI)

Intracellular Ca<sup>2+</sup> detection.

| Probe                | Origin              | Detection technique                 | Ref. |
|----------------------|---------------------|-------------------------------------|------|
| Aequorin             | Genetically encoded | Luminometry                         | 15   |
| Berovin              | Genetically encoded | Luminometry                         | 22   |
| Obelin               | Genetically encoded | Luminometry                         | 23   |
| Cameleon             | Genetically encoded | FRET microscopy                     | 24   |
| Troponin C biosensor | Genetically encoded | FRET microscopy                     | 25   |
| Camgaroo             | Genetically encoded | Fluorescence microscopy             | 26   |
| Ratiometric Pericam  | Genetically encoded | Ratiometric fluorescence microscopy | 27   |
| GEM-GECO1            | Genetically encoded | Ratiometric fluorescence microscopy | 28   |
| Calcium Green-1      | Synthetic           | Fluorescence microscopy             | 29   |
| Fluo-3, Fluo-4       | Synthetic           | Fluorescence microscopy             | 29   |
| Fura-2, Indo-1       | Synthetic           | Ratiometric fluorescence microscopy | 30   |



FRET-tandem probes  
modified to measure Ca<sup>2+</sup>

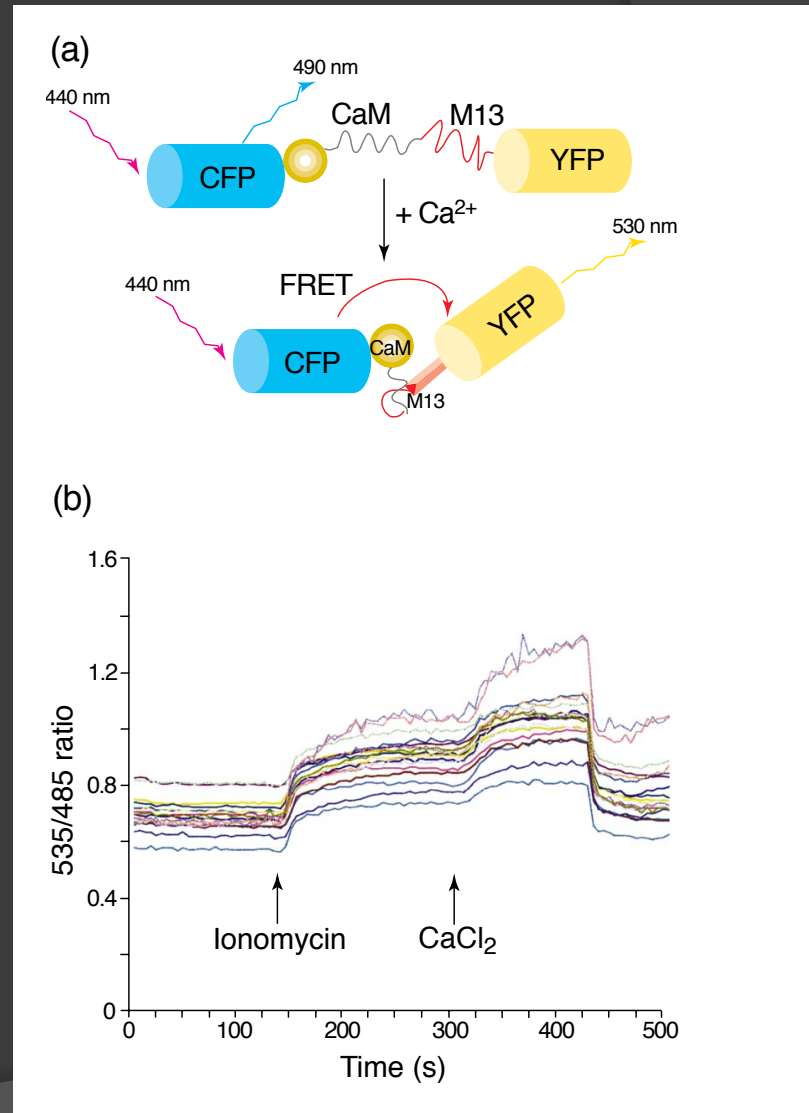


# Camaleons

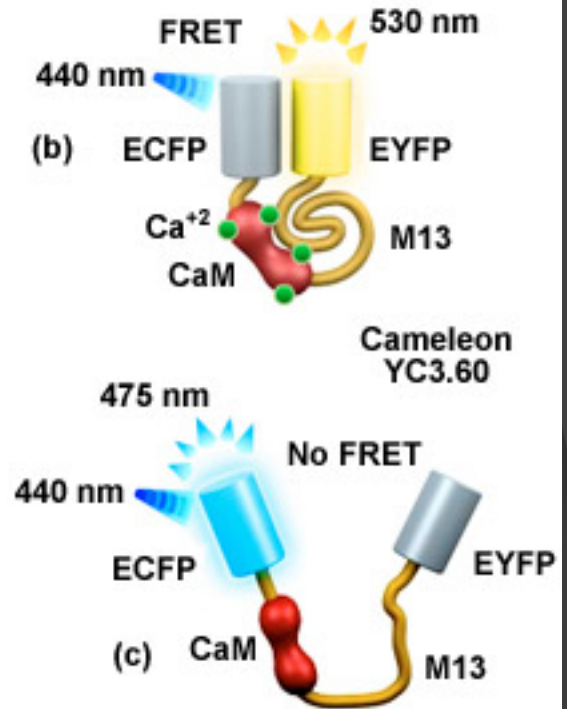
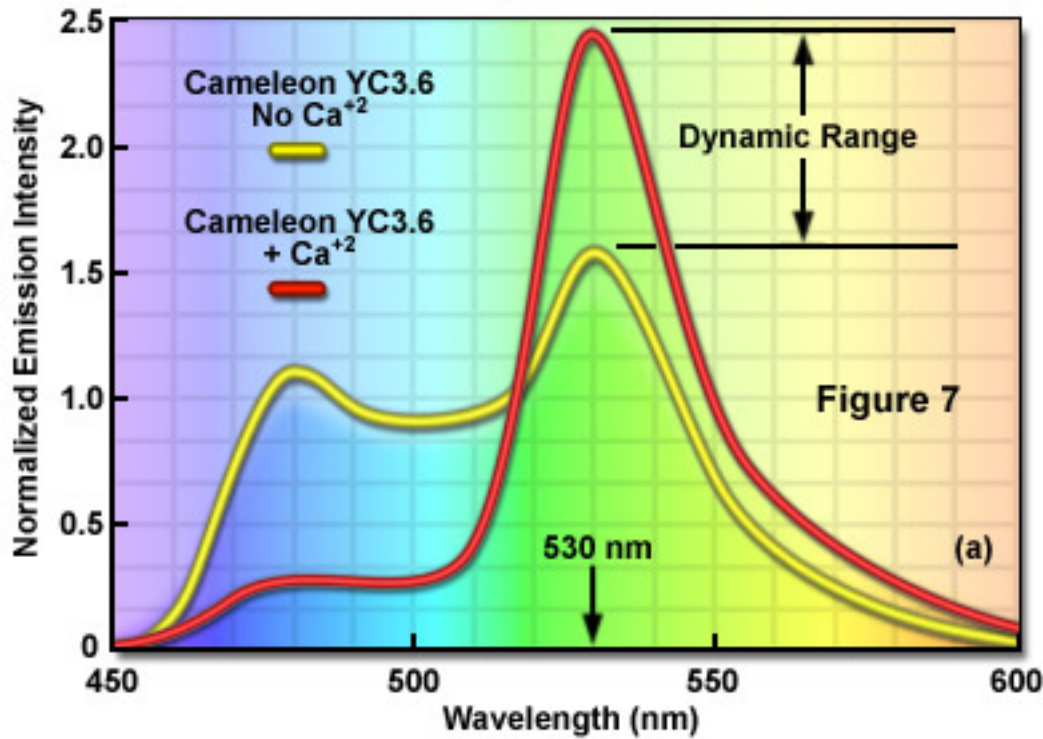
Cameleons are chimeric proteins consisting of a blue or cyan mutant of green fluorescent protein (GFP), calmodulin (CaM), a glycyglycine linker, the CaM-binding domain of myosin light chain kinase (M13), and a green or yellow version of GFP.

Ca<sup>2+</sup> binding to the CaM causes intramolecular CaM binding to M13.

The resulting change from an extended to a more compact conformation increases the efficiency of fluorescence resonance energy transfer between the shorter to the longer wavelength mutant GFP.



# Spectral Imaging with Fluorescent Protein FRET Biosensors

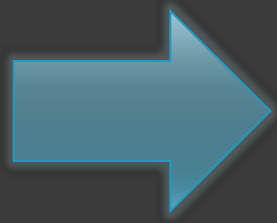


<http://zeiss.magnet.fsu.edu/tutorials/spectralimaging/spectralfret/indexflash.html>

# Camaleons

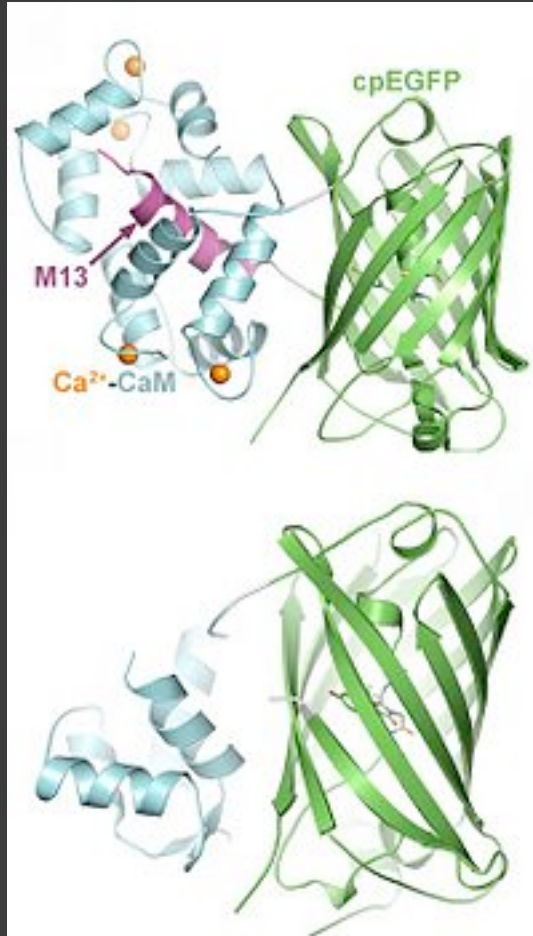
Because GFP fusions can be expressed *in situ*, they can be targeted to subcellular organelles such as the endoplasmic reticulum (ER), where there are  $\text{Ca}^{2+}$  stores. By adjusting the  $\text{Ca}^{2+}$  affinities through mutation of the calmodulin protein and establishing that the emission ratio correlated with  $\text{Ca}^{2+}$  concentration, the authors measured the free  $[\text{Ca}^{2+}]$  in both the cytoplasm and ER. They found that the free  $[\text{Ca}^{2+}]$  in the ER was 60–400  $\mu\text{M}$  in unstimulated cells, falling to 1–50  $\mu\text{M}$  in cells treated with  $\text{Ca}^{2+}$  ionophores (e.g. ionomycin).

# Genetically encoded $\text{Ca}^{2+}$ indicators (GECI)

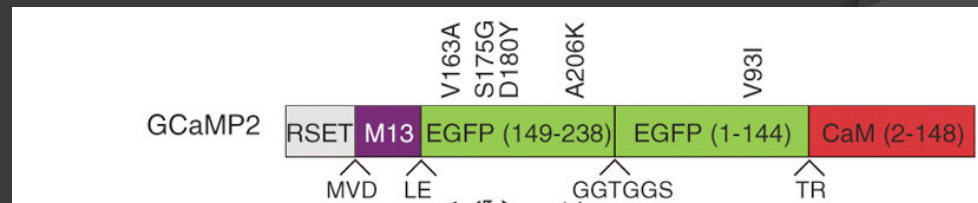
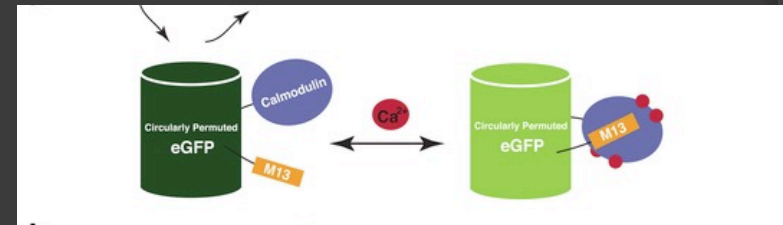


GCaMP

# GCaMP



- GCaMP is a genetically encoded, high-affinity  $\text{Ca}^{2+}$  sensor that exhibits large fluorescent shifts in response to physiological  $\text{Ca}^{2+}$  changes. The sensor comprises a circularly permuted EGFP (cpGFP) flanked by CaM and a CaM-binding peptide (M13) from myosin light chain kinase. Increases in  $\text{Ca}^{2+}$  promote  $\text{Ca}^{2+}$ -CaM-M13 interaction and a conformational change within the sensor, resulting in an increase in EGFP fluorescence



None of these protein-based indicators have yet surpassed the sensitivity and speed of commonly used synthetic calcium indicators (for example, Oregon Green Bapta-1-AM, OGB1-AM).

Therefore, depending on the experimental goals, investigators choose between sensitive synthetic indicators delivered by invasive chemical or physical methods, or less sensitive protein sensors delivered by genetic methods.

This is of particular interest mainly in neurons.

Because neurons have unusually fast calcium dynamics and low peak calcium accumulations, sensors designed to probe neuronal function are best tested in neurons rather than in non-neuronal systems, most of which show much slower and larger calcium changes.

Make sense therefore to screen GCaMP variants produced by mutagenesis in neurons, and subsequently validated lead sensors in several in vivo systems.

# Ultrasensitive fluorescent proteins for imaging neuronal activity

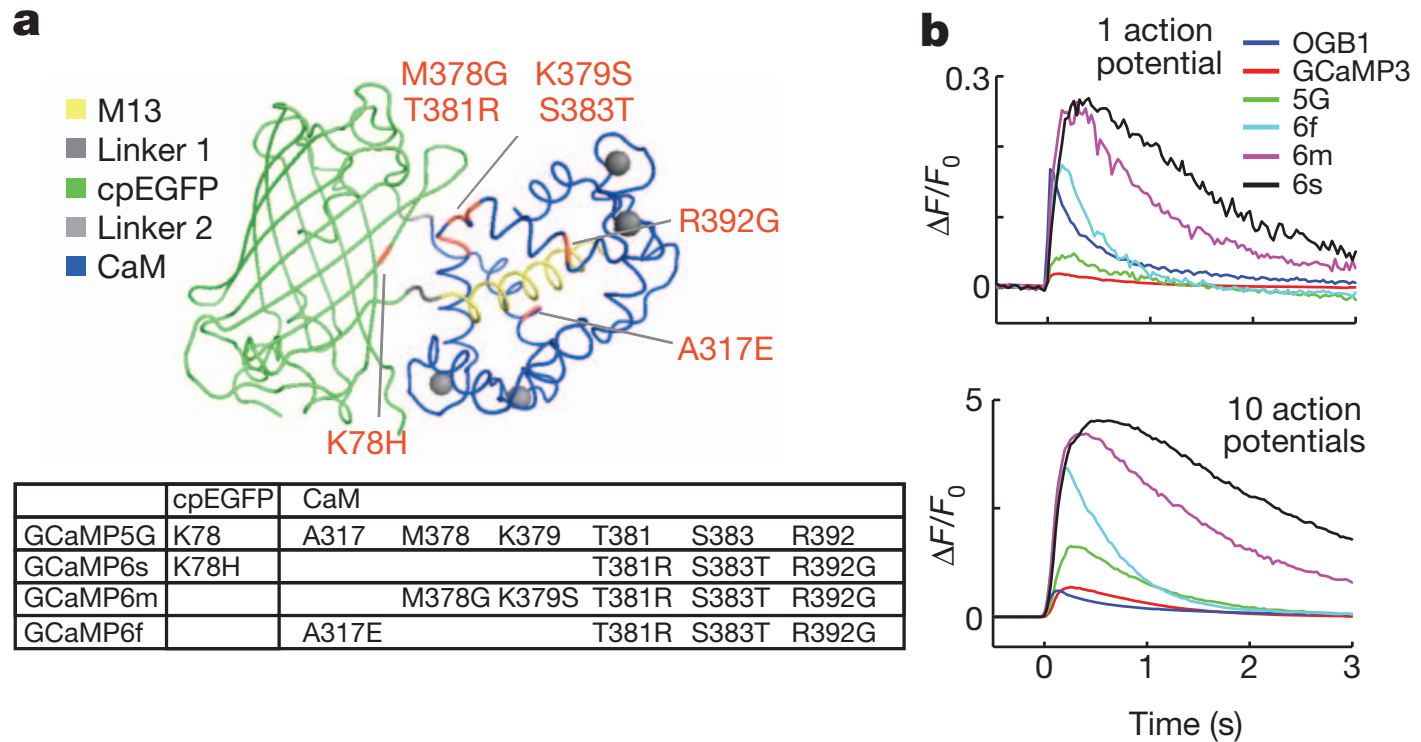
Tsai-Wen Chen<sup>1</sup>, Trevor J. Wardill<sup>1†</sup>, Yi Sun<sup>1</sup>, Stefan R. Pulver<sup>1</sup>, Sabine L. Renninger<sup>2</sup>, Amy Baohan<sup>1,3</sup>, Eric R. Schreiter<sup>1</sup>, Rex A. Kerr<sup>1</sup>, Michael B. Orger<sup>2</sup>, Vivek Jayaraman<sup>1</sup>, Loren L. Looger<sup>1</sup>, Karel Svoboda<sup>1</sup> & Douglas S. Kim<sup>1</sup>

18 JULY 2013 | VOL 499 | NATURE | 295

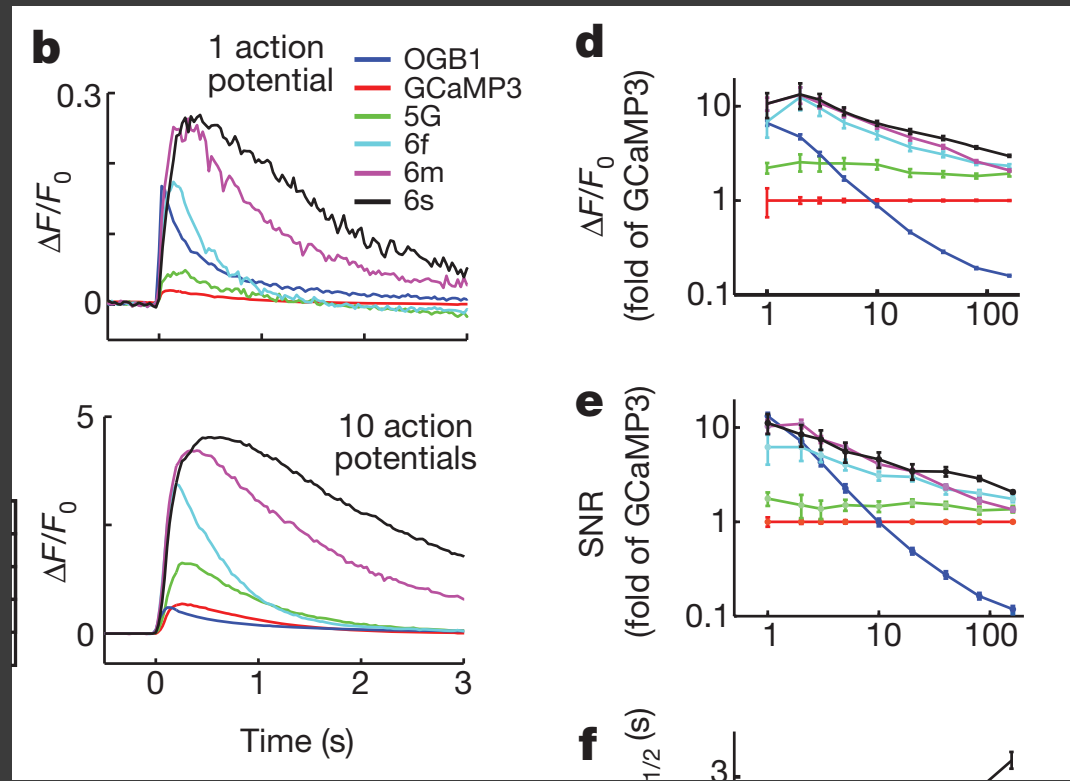
©2013 Macmillan Publishers Limited. All rights reserved

Despite extensive structure-guided optimization GCaMP and other protein sensors still suffer from low sensitivity and slow kinetics.





We produced numerous additional GCaMP variants and tested them in automated neuronal assays (Fig. 1). With the aim of improving sensitivity, we focused mutagenesis on the interface between cpGFP and CaM at 16 amino acid positions, some mutagenized to near completion (Fig. 1a). Mutations were made at 18 additional sites, notably at the M13–CaM interface which can affect calcium affinity (A317) and in CaM (R392) (Fig. 1a).



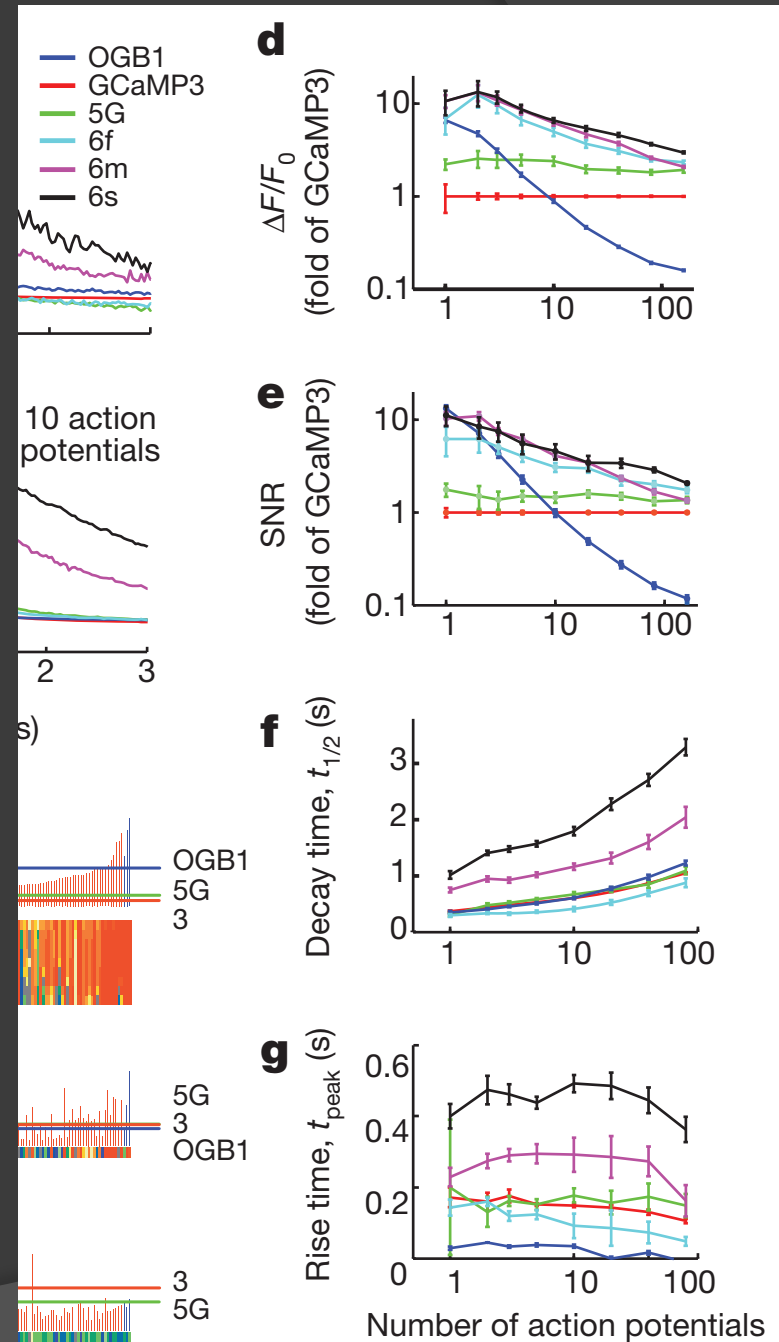
Dissociated rat hippocampal neurons in 24-well plates were transduced with GCaMP variants (one per well), together with nuclear mCherry, using lentivirus-mediated gene transfer. Electrodes triggered trains of action potentials in all neurons within each well.

Time-lapse images (35Hz) of 800  $\mu\text{m}$  fields of view containing 10–100 neurons were acquired, while delivering a series of action potential trains (Fig. 1b).

Fluorescence changes extracted from single neurons were used to compare the sensitivity, dynamic range and kinetics of individual GCaMP variants and OGB1-AM (Fig. 1b–g). We monitored the resting brightness of the sensor by measuring green fluorescence relative to red mCherry fluorescence.

In total, we screened 447 GCaMP variants (Supplementary Table 5).

Based on screening in cultured neurons (Fig. 1), we chose three ultrasensitive GCaMP6 sensors (GCaMP6s, 6m, 6f; for slow, medium and fast kinetics, respectively) for characterization in vivo.

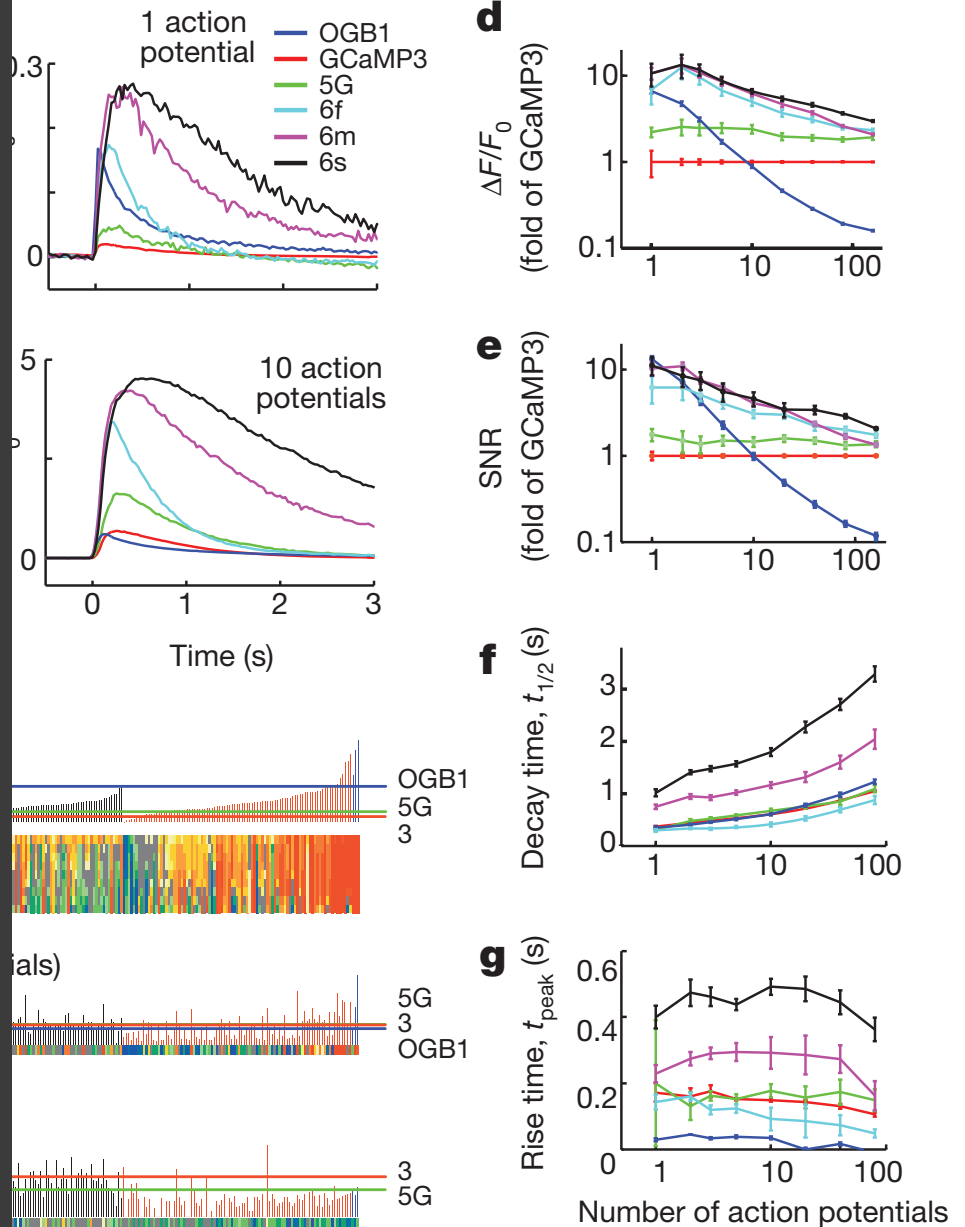


Compared to GCaMP5G, the GCaMP6 sensors have similar baseline brightness and a 1.1- to 1.6-fold increase in dynamic range ( $\Delta F/F_0$  at 160 action potentials).

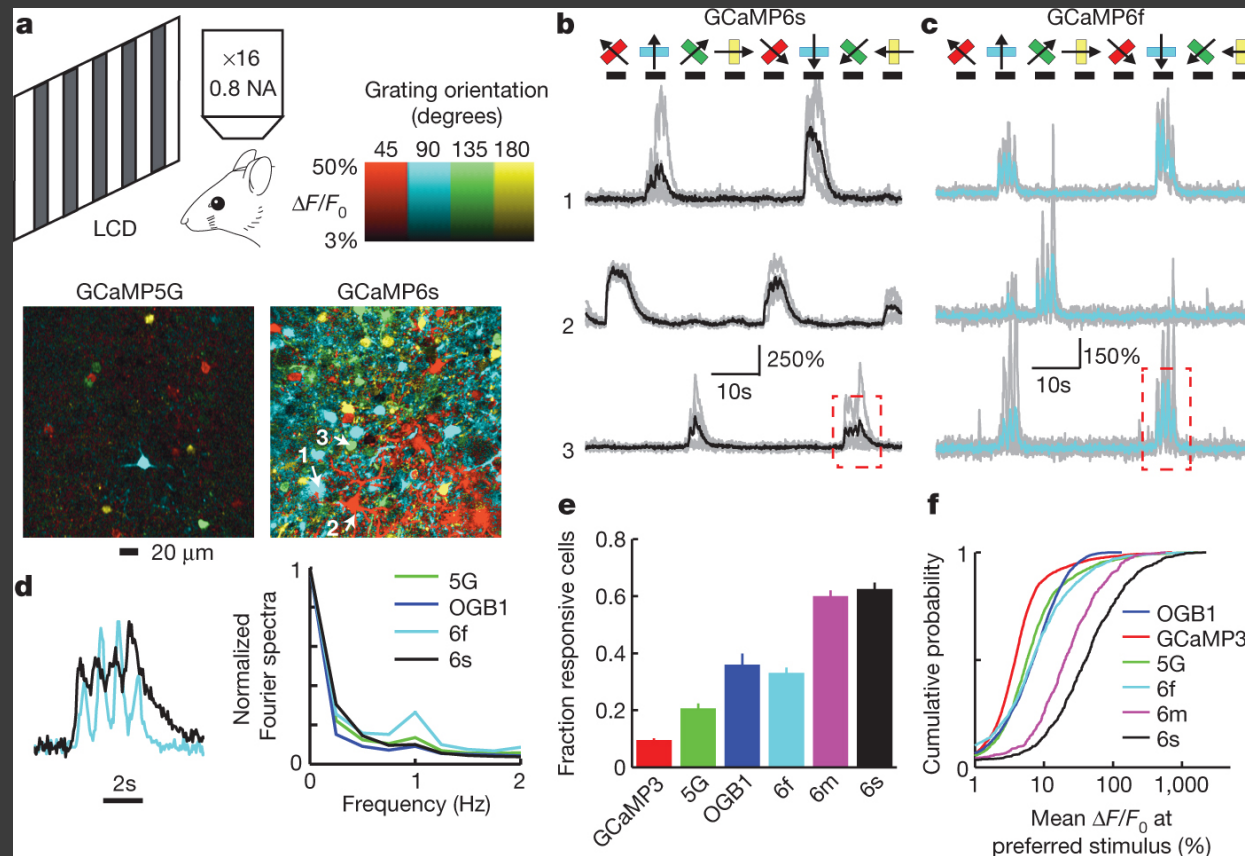
For small numbers of action potentials the most sensitive sensor, GCaMP6s, produced sevenfold larger signals (10-fold larger than GCaMP3, Fig. 1b–e).

The fastest sensor, GCaMP6f, had two fold faster rise time and 1.7-fold faster decay time than GCaMP5G (Fig. 1f, g).

**GCaMP6f** is the fastest genetically-encoded calcium indicator for cytoplasmic free calcium in neurons, with sensitivity comparable to OGB1-AM (Fig. 1d–g).

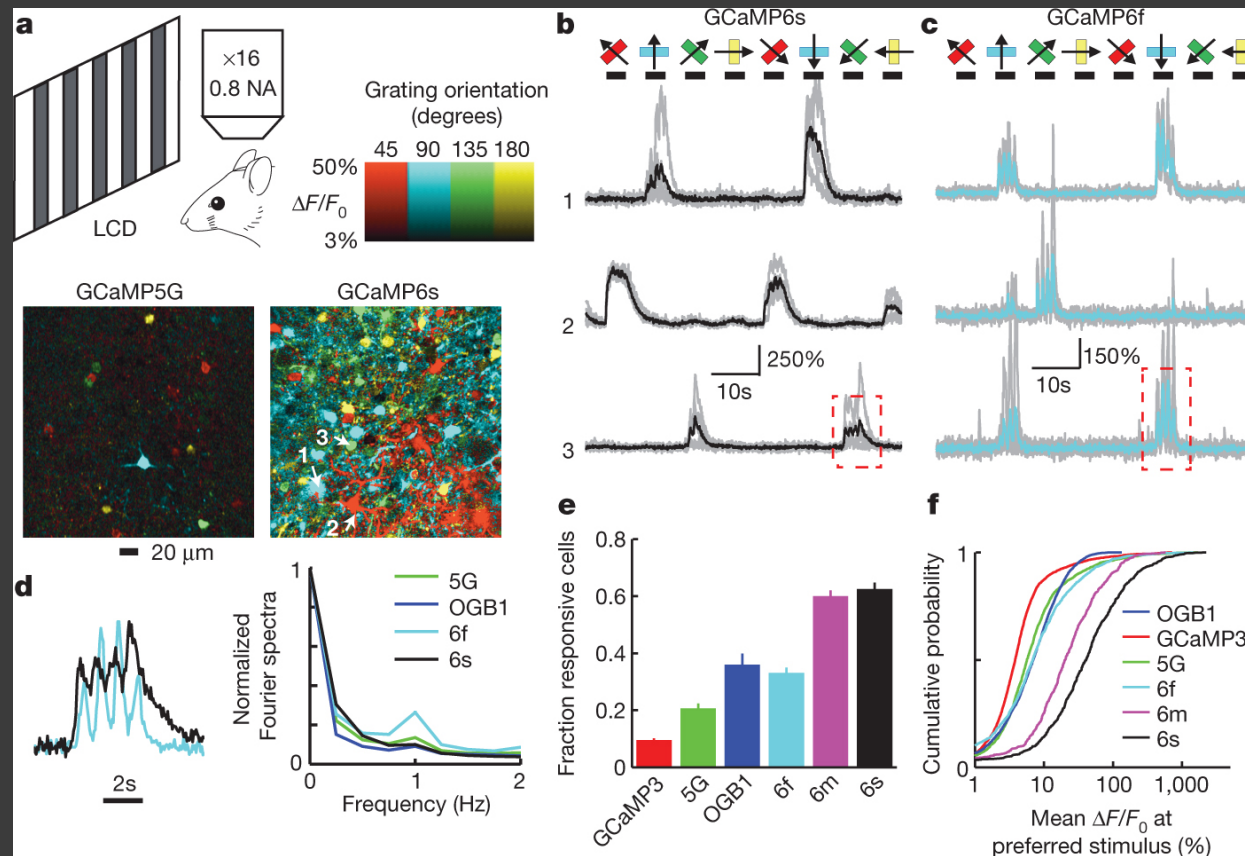


# GCaMP6 performance in the mouse visual cortex.



We next tested GCaMP6 in layer (L) 2/3 pyramidal neurons in the mouse visual cortex V1 in vivo. V1 was infected with adeno-associated virus (AAV) expressing GCaMP variants (AAV-hsyn1-GCaMP variant). Three weeks after AAV infection, the vast majority of L2/3 neurons showed fluorescence mainly in the neuronal cytoplasm

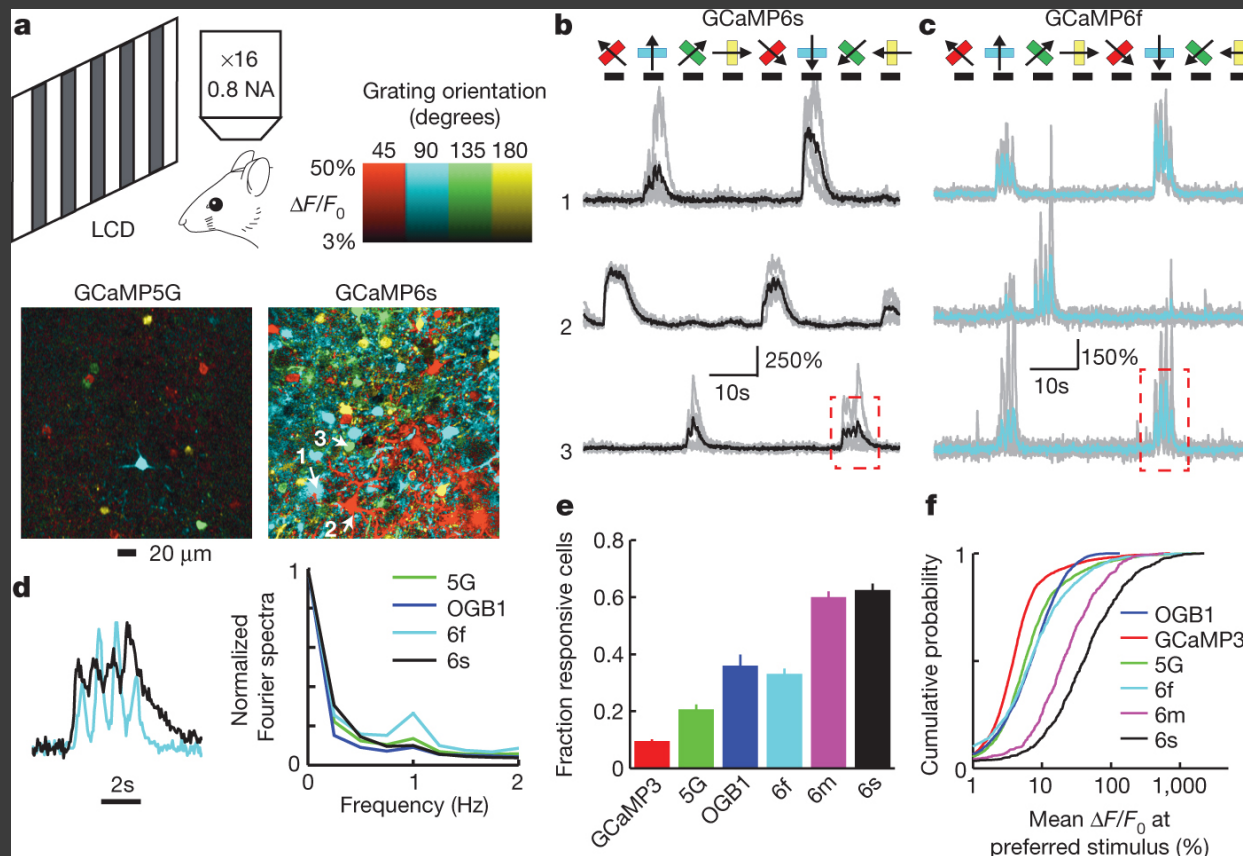
# GCaMP6 performance in the mouse visual cortex.



Sensory stimuli consisted of moving gratings presented in eight directions to the contralateral eye. Two-photon imaging revealed visual stimulus-evoked fluorescence transients in subsets of neurons (Fig. 2a–c). Fluorescence transients were faster with GCaMP6f compared to other sensors and faithfully tracked dynamic sensory stimuli (Fig. 2d).

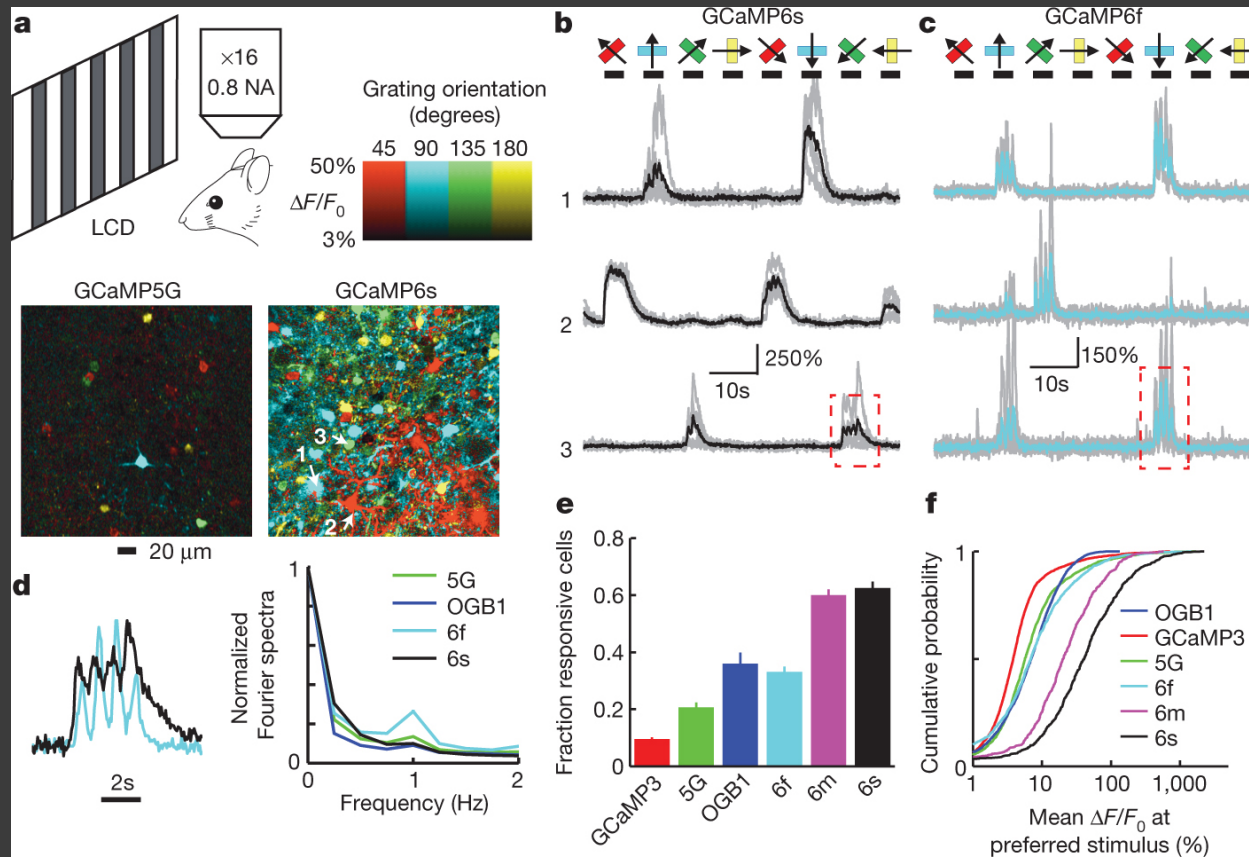


# GCaMP6 performance in the mouse visual cortex.



GCaMP6 performance was compared to other sensors in several ways. The fraction of responding neurons detected with GCaMP6s was threefold higher than for GCaMP5G (fivefold higher than GCaMP3) (Fig. 2e). Notably, the fractions of active neurons detected with GCaMP6s and GCaMP6m were also significantly higher than for OGB1-AM (Fig. 2e, f,  $P < 0.01$ , Wilcoxon rank sum test). GCaMP6 sensors thus reveal neuronal dynamics that were previously undetectable with protein sensors.

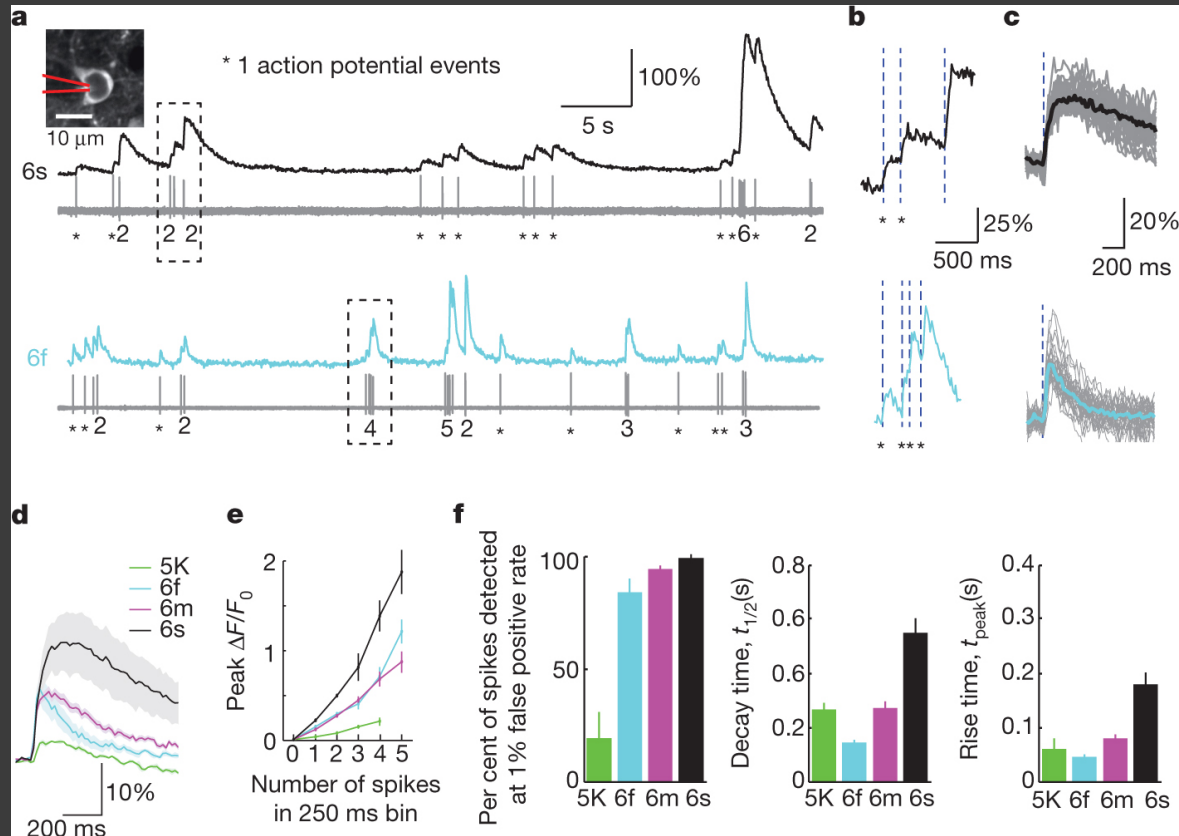
# GCaMP6 performance in the mouse visual cortex.



GCaMP6 sensors thus reveal neuronal dynamics that were previously undetectable with protein sensors.



# Combined imaging and electrophysiology in the visual cortex.

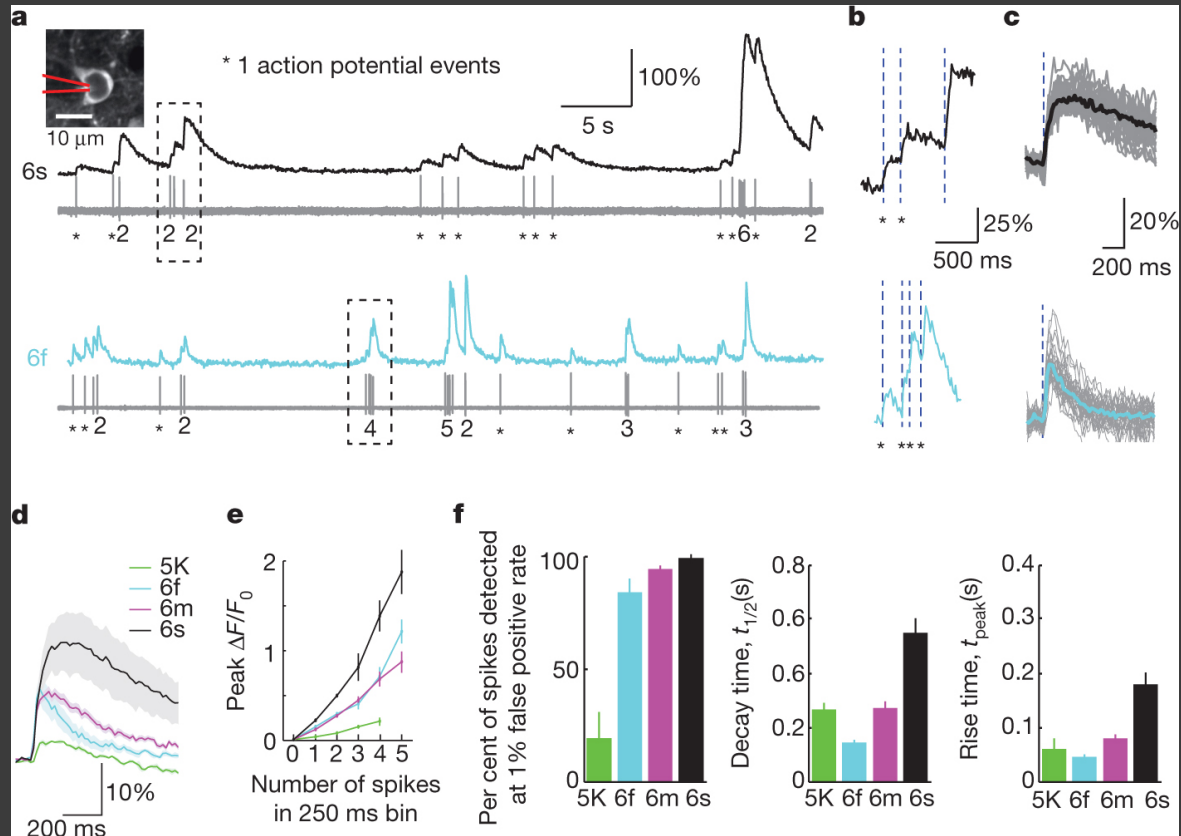


We directly compared cellular fluorescence changes and spiking using loose-seal, cell-attached recordings. GCaMP6s produced large fluorescence transients even in response to single action potentials (.6 times larger than for GCaMP5K, Fig. 3 and Supplementary Video 1), yielding high detection rates for single spikes.

20%  
0.5mV  
1s

10  $\mu\text{m}$

# Combined imaging and electrophysiology in the visual cortex.



GCaMP6f and GCaMP6m showed slightly lower spike detection efficiencies, but with faster kinetics (Fig. 3). Individual spikes within a burst resulted in stepwise fluorescence increases (Fig. 3b), which were resolvable if they were separated by an interval on the order of the rise time of the sensor or more (100–150ms, GCaMP6s; 75–100 ms, GCaMP6m; 50–75ms, GCaMP6f).

GCaMP6 indicators cross important performance thresholds. They have higher sensitivity than commonly used synthetic calcium dyes (for example, OGB1-AM) and detect individual action potentials with high reliability at reasonable microscope magnifications. These indicators can be used to image large groups of neurons as well as tiny synaptic compartments over multiple imaging sessions separated by months. It is likely that these sensors will find widespread applications for diverse problems in brain research and calcium signalling.

## Imaging Neural Activity Using *Thy1*-GCaMP Transgenic Mice

Qian Chen,<sup>1</sup> Joseph Cichon,<sup>3,10</sup> Wenting Wang,<sup>1,10</sup> Li Qiu,<sup>4</sup> Seok-Jin R. Lee,<sup>4</sup> Nolan R. Campbell,<sup>1</sup> Nicholas DeStefino,<sup>6</sup> Michael J. Goard,<sup>2</sup> Zhanyan Fu,<sup>1,5</sup> Ryohei Yasuda,<sup>4</sup> Loren L. Looger,<sup>7</sup> Benjamin R. Arenkiel,<sup>8</sup> Wen-Biao Gan,<sup>3</sup> and Guoping Feng<sup>1,9,\*</sup>

<sup>1</sup>McGovern Institute for Brain Research, Department of Brain and Cognitive Sciences

<sup>2</sup>Picower Institute for Learning and Memory, Department of Brain and Cognitive Sciences  
Massachusetts Institute of Technology, Cambridge, MA 02139, USA

<sup>3</sup>Molecular Neurobiology Program, Skirball Institute, Department of Physiology and Neuroscience, New York University School of Medicine, New York, NY 10016, USA

<sup>4</sup>Department of Neurobiology

<sup>5</sup>Department of Psychiatry and Behavioral Science  
Duke University Medical Center, Durham, NC 27710, USA

<sup>6</sup>MD-PhD Program, Harvard Medical School, Boston, MA 02115, USA

<sup>7</sup>Howard Hughes Medical Institute, Janelia Farm Research Campus, Ashburn, VA 20147, USA

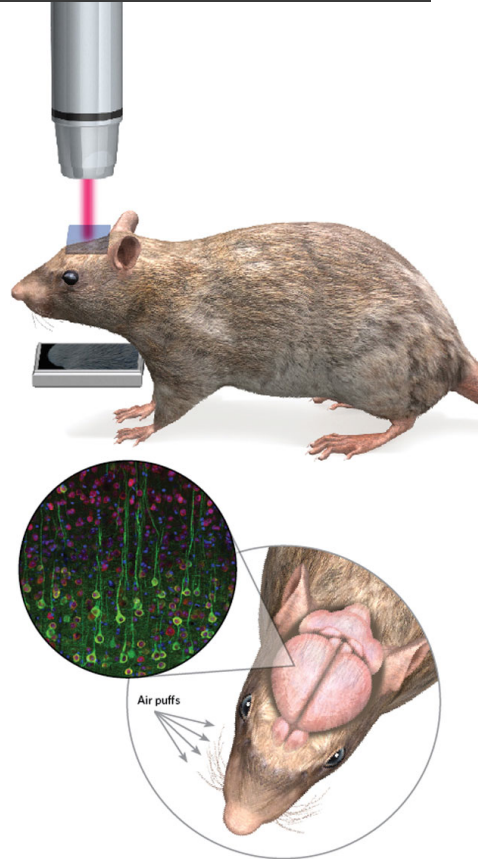
<sup>8</sup>Department of Molecular and Human Genetics, Baylor College of Medicine, Houston, TX 77030, USA

<sup>9</sup>Stanley Center for Psychiatric Research, Broad Institute, Cambridge, MA 02142, USA

<sup>10</sup>These authors contributed equally to this work

\*Correspondence: [fengg@mit.edu](mailto:fengg@mit.edu)

<http://dx.doi.org/10.1016/j.neuron.2012.07.011>





ARTICLE

DOI: 10.1038/s41467-018-03719-6

OPEN

# Improved calcium sensor GCaMP-X overcomes the calcium channel perturbations induced by the calmodulin in GCaMP

Yaxiong Yang <sup>1,2,3,4</sup>, Nan Liu<sup>1,7</sup>, Yuanyuan He<sup>1</sup>, Yuxia Liu<sup>1</sup>, Lin Ge<sup>1</sup>, Linzhi Zou<sup>5</sup>, Sen Song<sup>1,4</sup>, Wei Xiong<sup>4,5</sup> & Xiaodong Liu <sup>1,2,3,4,5,6</sup>

....In practice GCaMP reportedly causes unexpected and unwanted “side-effects” in multiple aspects. The major concern is about cell damages induced by GCaMP. For instance cytotoxicity or death in neurons.

These side-effects seem to be closely associated with abnormal accumulation of GCaMP filling in the nuclei, often accompanied by attenuation and/or distortion of  $\text{Ca}^{2+}$  dynamics as evidenced in neurons.

Another line of evidence, comes from functional studies reporting the alterations of physiological  $\text{Ca}^{2+}$  and intrinsic excitability, e.g., gain of function in firing rates was observed from hippocampal neurons of GCaM5G transgenic mice. And recently, multiple lines of GCaMP6 mice are reported to exhibit major abnormalities in their brain activity.

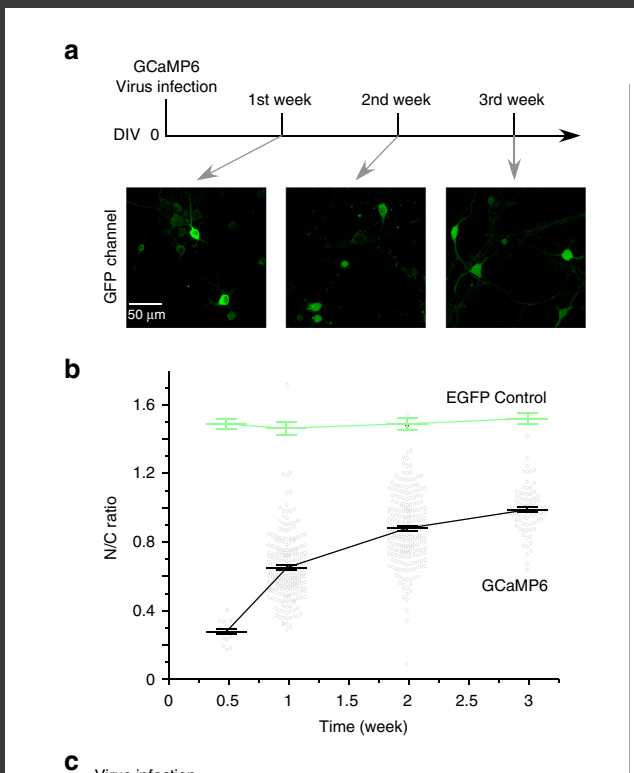
CaM is ubiquitous signal protein in cells acting as either apoCaM (Ca<sup>2+</sup>-free CaM) or calcified CaM (Ca<sup>2+</sup>/CaM). Ca<sup>2+</sup>/CaM is widely involved in numerous Ca<sup>2+</sup>-signaling cascades including gene transcription; and apoCaM also regulates the functions of diverse proteins including ion channels.

We suspect that the problems of GCaMP might be due to its potential perturbations of signaling networks and normal protein functions pertaining to CaM.



We newly developed **GCaMP-X** as our solution, by engineering an additional apoCaM-binding motif and an extra tag ensuring subcellular localization into conventional GCaMP.

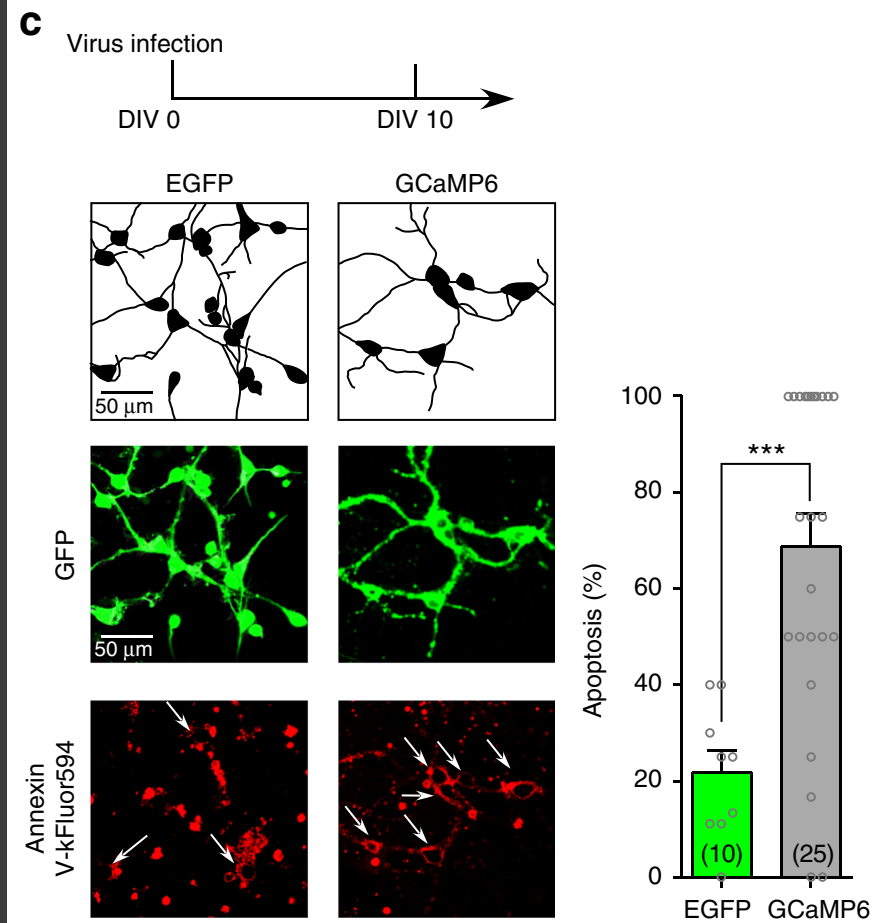




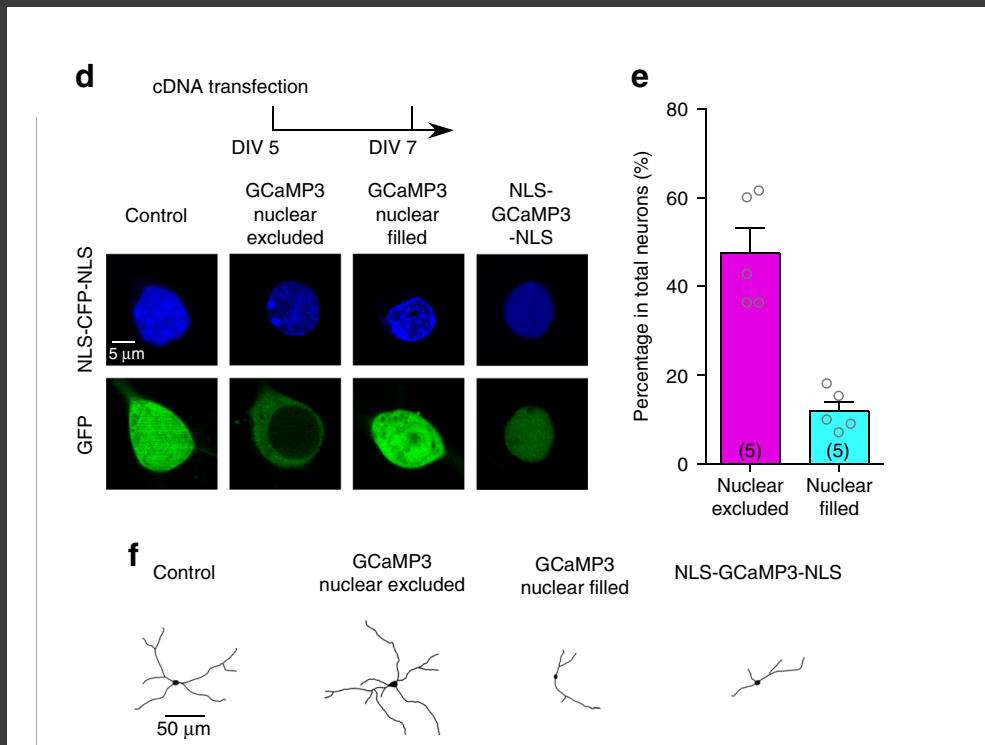
Cellular model: cortical neurons infected with AAV-syn-GCaMP6f virus (Fig. 1a). In contrast to stable EGFP control, **GCaMP6f** exhibited a time-dependent trend of **accumulation in the nucleus**, which started with N/C (nuclear/cytosolic) ratio of  $0.29 \pm 0.02$  ( $n = 16$ ) in half a week, but gradually reaching  $0.99 \pm 0.01$  ( $n = 82$ ) at the timepoint of 3rd week (Fig. 1b).

Such aberrant nuclear accumulation of GCaMP is reportedly problematic, usually accompanied by various side-effects.

As demonstrated by the apoptosis assay (Annexin V kit), at the time of 10th day (GCaMP N/C ratio of  $\sim 0.8$ ) robust signals of apoptosis were detected from a large fraction ( $>60\%$ ) of neurons infected with AAV-Syn-GCaMP6f virus (Fig. 1c), whereas much less for control neurons infected with AAV-Syn-EGFP ( $\sim 20\%$ ).



we examined and quantified the cytonuclear distribution of GCaMP in relation to neurite out-growth.

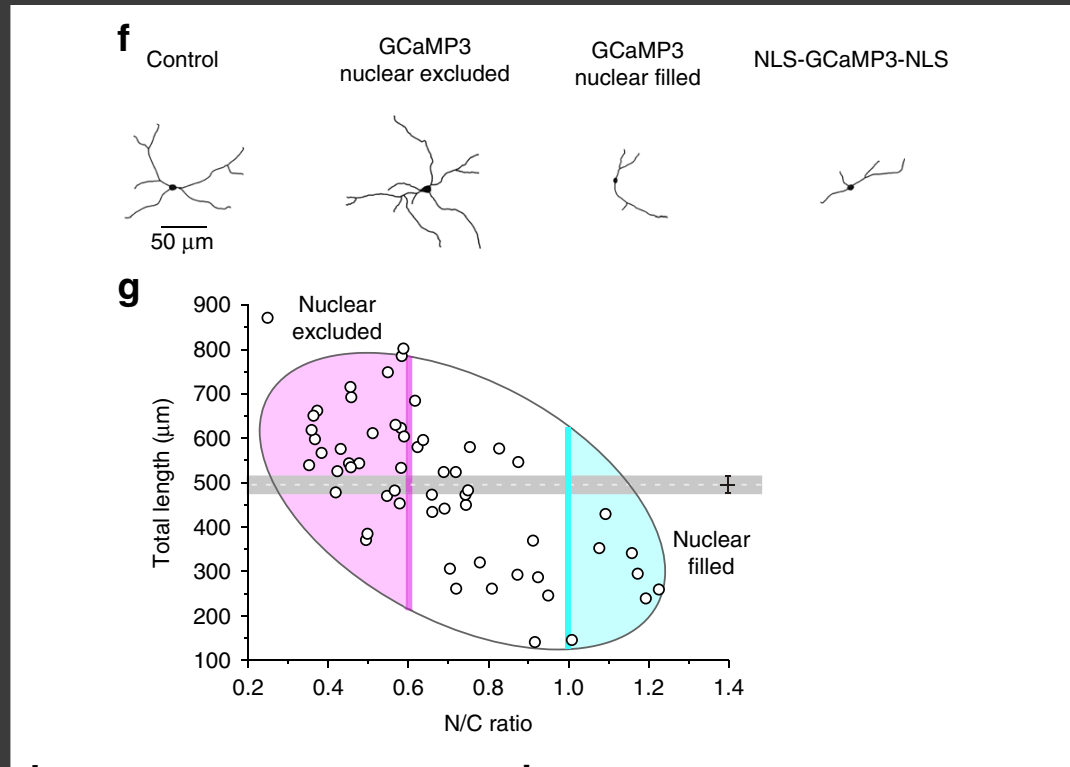


GCaMP3 distributions can be segregated into two extreme patterns by the criteria of N/C ratio of GCaMP3 fluorescence:

- nuclear-excluded (N/C ratio  $< 0.6$ , ~50% out of the total number of neurons)
- nuclear-filled (N/C ratio  $> 1$ , ~10% of neurons) (Fig. 1d, e).

We then examined the potential neural damages due to nuclear accumulation of GCaMP, by tracing the neurite morphology indicated by green fluorescence in each neuron with the aid of wide-field confocal microscopy when necessary (Fig. 1d, f).

N/C ratio of GCaMP3 and the total length of neurites were calculated and correlated for individual neurons (Fig. 1g).



Nuclear-filled neurons were subject to significant reduction in neurite length compared to control neurons (Fig. 1g, horizontal line in grey), indicative of neural damages.

Thus, a **strong (negative) correlation** was clearly formed between N/C ratio of GCaMP3 and the total neurite length per neuron (Fig. 1g).

# GCaMP perturbs CaV1.3 gating.

Prior studies suspect that CaM contained in all versions of GCaMP might be one factor responsible for various side-effects.

However, it has been mostly attributed to **trivial reasons, such as buffering effects of Ca<sup>2+</sup>-binding CaM** one general concern common to any kind of Ca<sup>2+</sup> (binding).

In literature there are few evidences that **GCaMP might perturb CaM in CaV1 gating**, and thus CaV1-dependent signaling (e.g., excitation–transcription coupling).

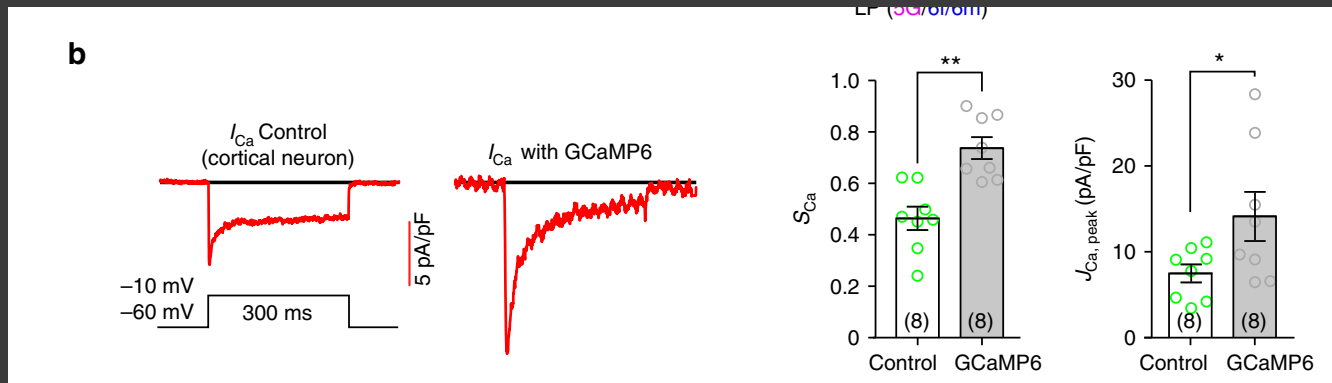
CaV1.3 is one major subtype of CaV1 channels expressed in neurons and tightly coupled to transcriptional signaling in the nucleus.

Also, CaV1-mediated E–T coupling could control neurite outgrowth.

CaV1.3 is subject to apoCaM tuning.

# GCaMP perturbs CaV1.3 gating.

We directly compared native ICa of cortical neurons (mostly mediated by CaV1.3 in our protocol) between the control group and GCaMP6f group by whole-cell patch-clamp recording (Fig. 2b).



**ICa recorded from GCaMP6f-overexpressing neurons was significantly different from the control, in that both CDI ( $S_{Ca}$ ) and VGA ( $J_{Ca}$ ) were augmented as shown by larger and “sharper” ICa traces at -10 mV, raising serious concerns that GCaMP would perturb native CaV1 in neurons.**

**GCaMP perturbs CaV1.3 gating.**

**In summary, GCaMP acts like CaM but with aberrant apoCaM and Ca<sup>2+</sup>/CaM functionalities, suggested by GCaMP perturbations on CaV1.3 gating.**

# GCaMP intervenes with excitation–transcription coupling.

The excitation–transcription coupling is highly specific to CaV1 in complex with CaM, which starts from CaV1 activities, followed by Ca<sup>2+</sup> binding to CaM proteins including the pre-associated CaM on the carboxyl terminus, Ca<sup>2+</sup>/CaM signaling back to the channel (such as CDI), Ca<sup>2+</sup>/CaM activation of CaMKII (CaM-dependent kinase II), CaM and CaMKII translocation to the nucleus, activation of nuclear CaM-dependent kinases and phosphorylation of CREB, eventually to gene transcription

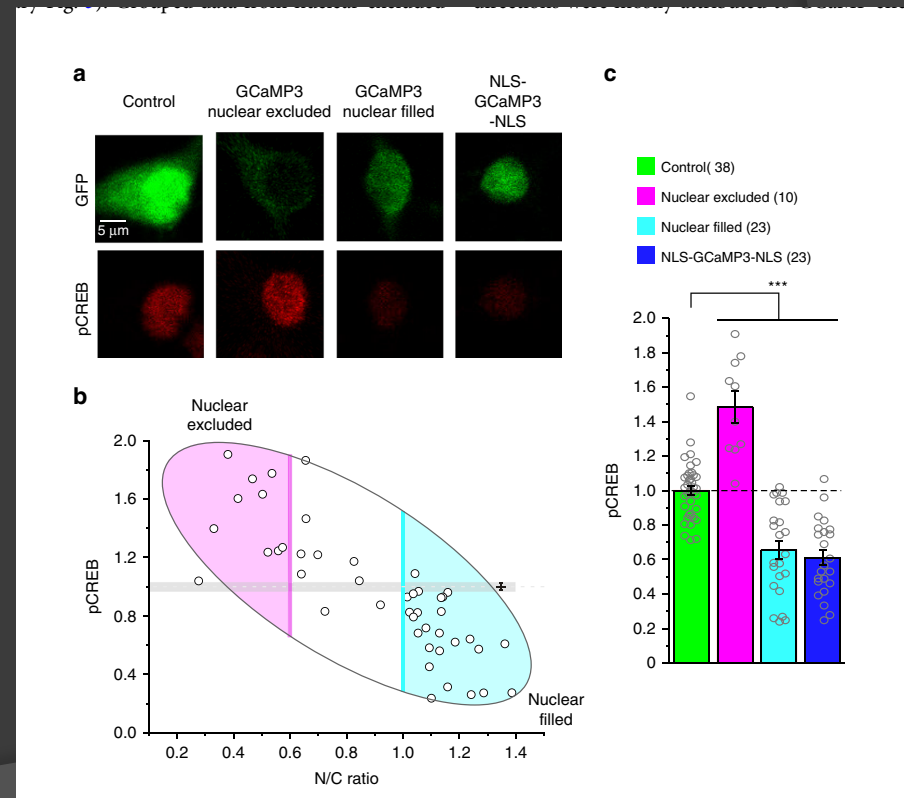


# GCaMP intervenes with excitation–transcription coupling.

GCaMP perturbs the gating of CaV1/CaM complex (Fig. 2), and may also affect the downstream signals along the E–T pathway.

We examined the level of phosphorylated CREB (pCREB) in cultured cortical neurons expressing GCaMP3 of different distributions

Normalized pCREB of GCaMP3-expressing neurons exhibited strong (negative) correlations with the N/C ratio (Fig. 3b) of GCaMP. pCREB signals under normal physiological conditions (control group) were significantly decreased by nuclear GCaMP3 but aberrantly enhanced by cytosolic GCaMP3 (Fig. 3c),



# GCaMP intervenes with excitation–transcription coupling.

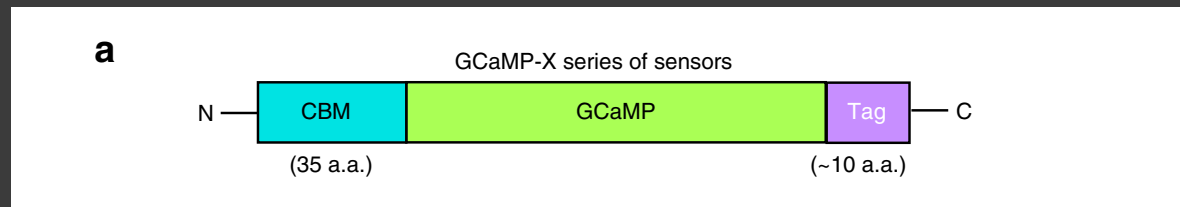
...Particularly, GCaMP present in the nucleus could severely impair pCREB signaling by dominant negative effects of aberrant CaM-like activities, considering that CaM and CaM-interacting proteins plays important roles in nuclear signaling, many of which still await to uncover.

# Principles and implementations of GCaMP-X design

The apoCaM binding onto CaV1 channels appeared to be the first and probably also the central problem. As the potential solution, after a trial-and-error process, we came up with the design of GCaMP-X by introducing an extra motif of apoCaM protection, originated from the IQ domain (dynamic CaM-binding domain) of neuromodulin (GAP-43).

The protection motif was optimized to constitutively bind apoCaM with high affinity ( $K_d \approx 2 \mu\text{M}$ ), but bind  $\text{Ca}^{2+}/\text{CaM}$  with much lower affinity ( $K_d = 2 - 40 \mu\text{M}$ ) than M13 and other  $\text{Ca}^{2+}/\text{CaM}$  targets.

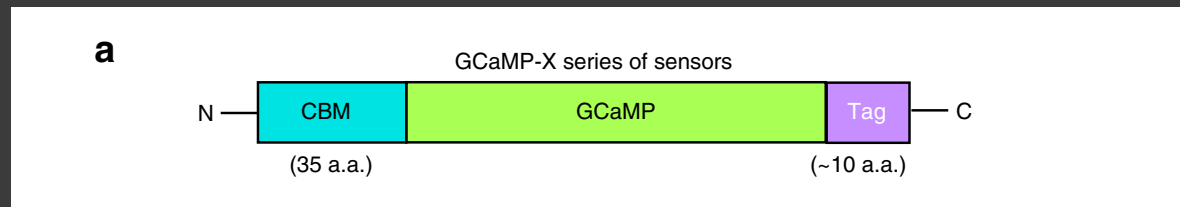
Such apoCaM binding motif (CBM) was fused onto the N-terminus of conventional GCaMP.



# Principles and implementations of GCaMP-X design

At rest, CBM/apoCaM would form the complex thus eliminating the interferences with gating and signaling of CaV1/CaM complex. When Ca<sup>2+</sup> rises, high-affinity M13, but not CBM, would bind Ca<sup>2+</sup>/CaM, relieving the concern that Ca<sup>2+</sup> sensing performance would be impaired by adding CBM.

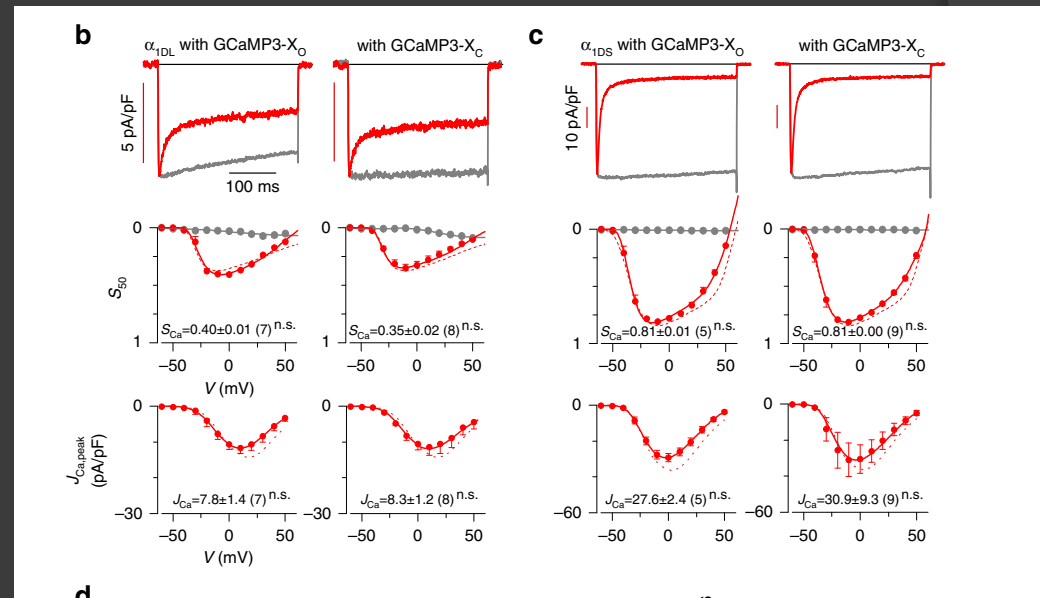
In addition to GCaMP-XO without any tag of localization signals, considering the particular importance of GCaMP distribution, **we appended short tags** onto the terminus of conventional GCaMP explicitly targeting different subcellular compartments (cytosol, membrane, and nucleus)



# Principles and implementations of GCaMP-X design

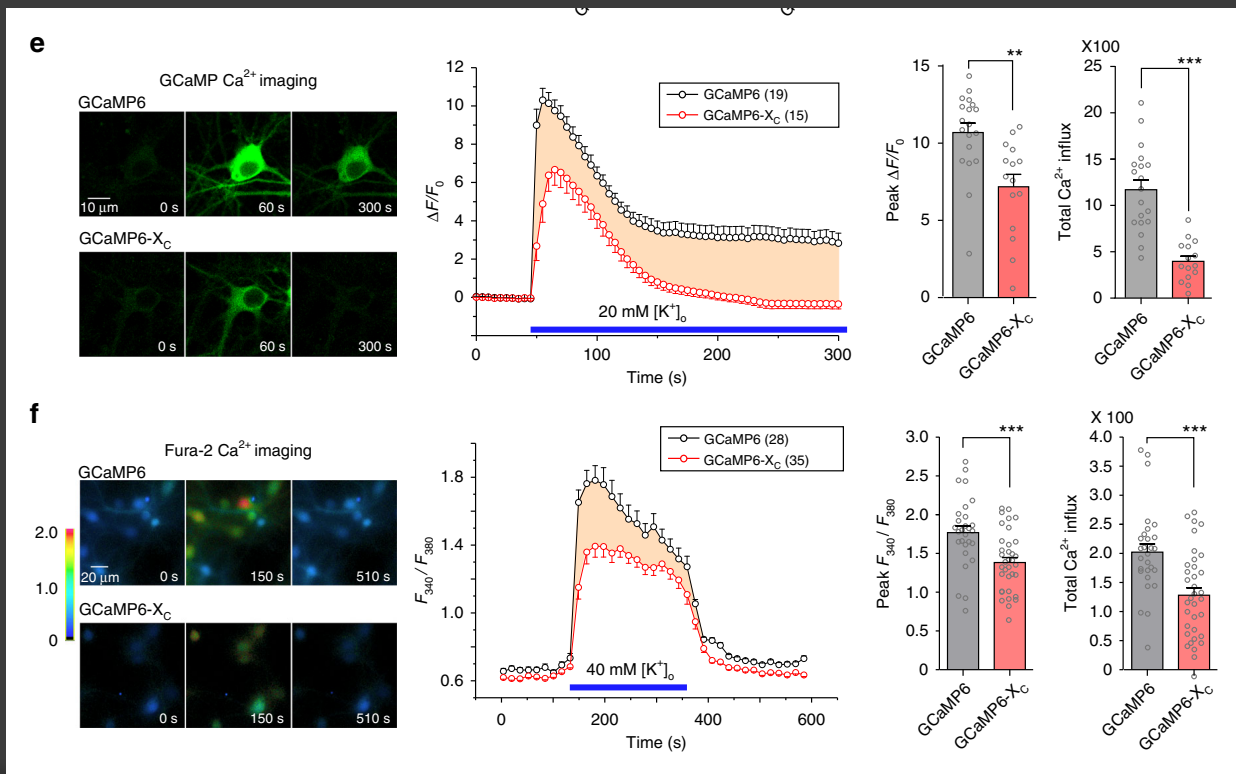
To validate such design, the prototypes of new sensors were coexpressed with CaV1.3, in hope to alleviate the interference with its gating (4b, 4c).

With GCaMP3-XO or GCaMP3-XC being present,  $\alpha$ 1DL or  $\alpha$ 1DS channels behaved indistinguishably from the control (no coexpression of sensors). Their comparable values of S<sub>Ca</sub> (CDI) and J<sub>Ca</sub> (VGA) indices confirmed successful isolation of the sensors from CaV1.



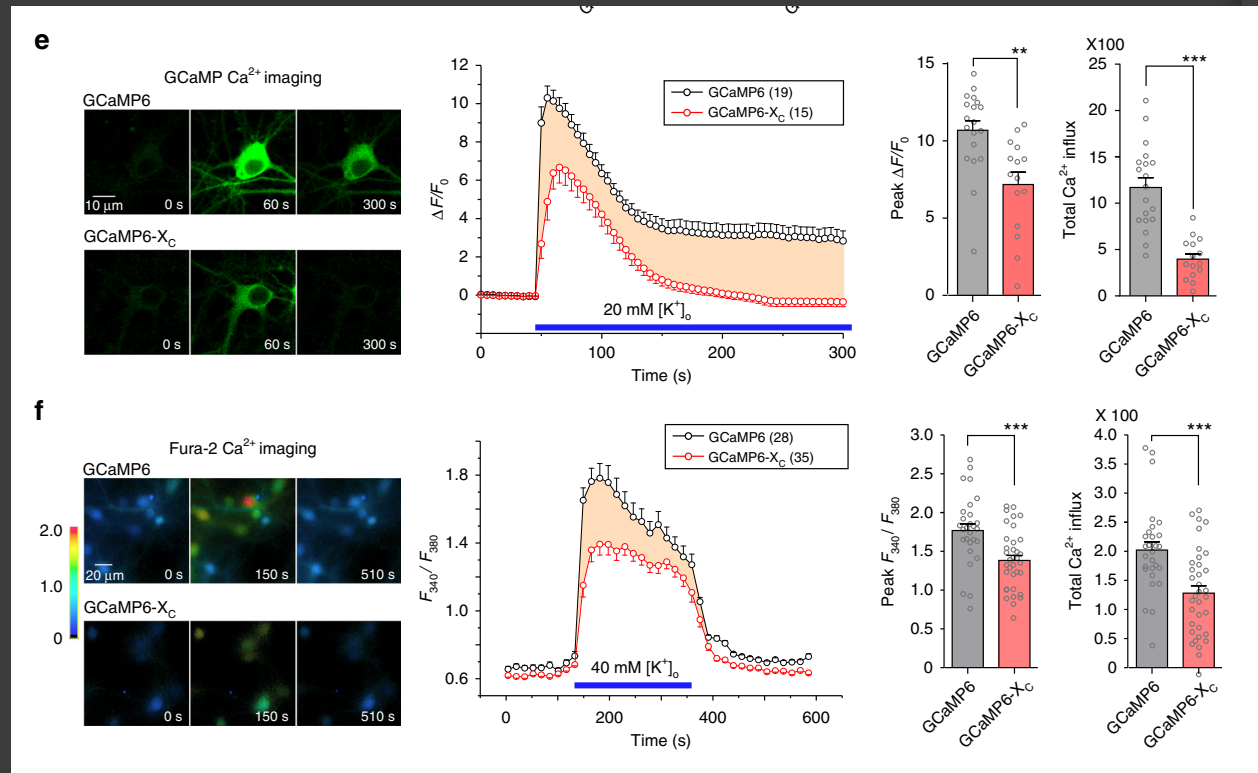
# Principles and implementations of GCaMP-X design

In addition, ratiometric Ca<sup>2+</sup> fluorescence imaging with Fura-2 (5  $\mu$ M) was performed, where F<sub>340</sub>/F<sub>380</sub> ratio (F<sub>340</sub> and F<sub>380</sub>, the fluorescence intensities of Fura-2 at excitation wavelength of 340 nm or 380 nm) was quantified as the index of (relative) Ca<sup>2+</sup> concentration.



# Principles and implementations of GCaMP-X design

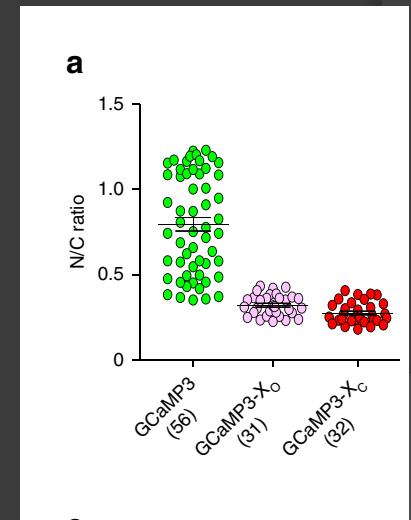
Upon 40 mM  $[K^+]_o$  applied to neurons, conventional GCaMP resulted into aberrantly higher  $Ca^{2+}$  signals than GCaMP6m-XC (Fig. 4f).



# GCaMP-X no longer perturbs CaV1 signaling in neurons.

Subsequent to validation of GCaMP-X in the aspects of CaV1 gating, we examined the side-effects of conventional GCaMP on other processes of E–T coupling in cortical neurons.

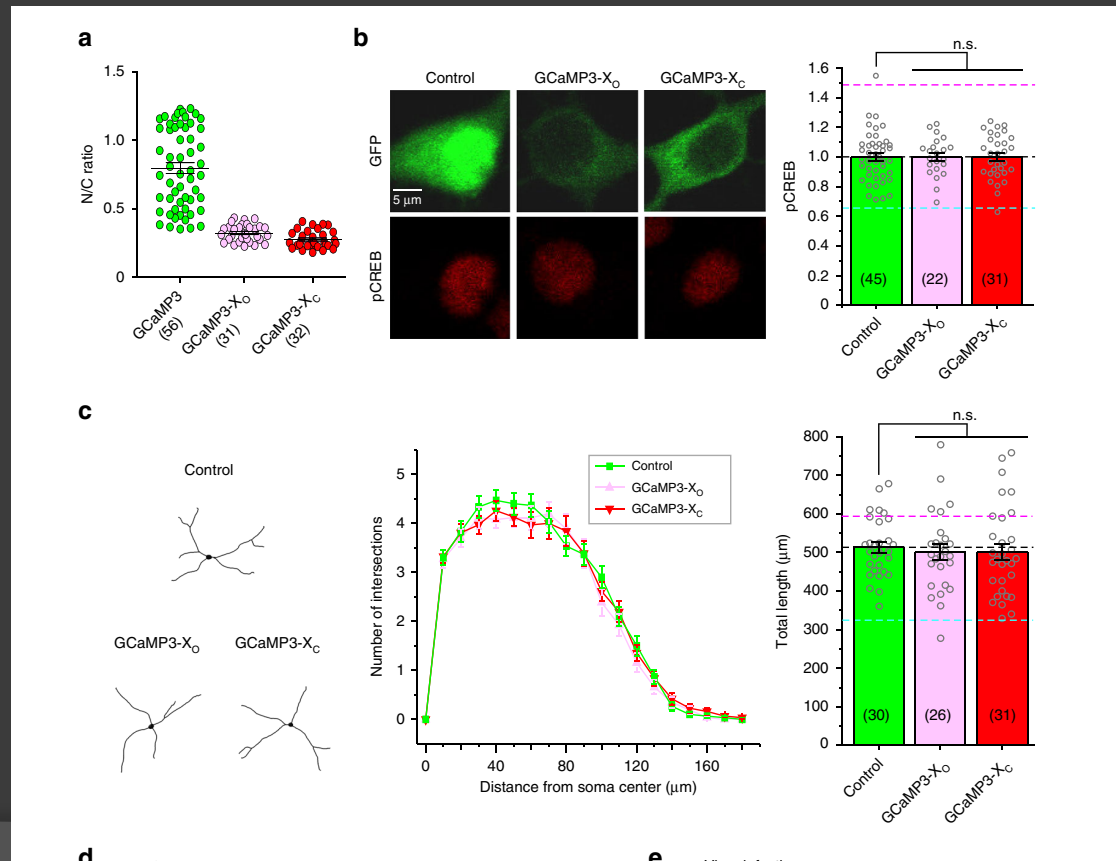
Distribution analysis indexed with N/C ratio for GCaMP3, GCaMP3-XO, and GCaMP3-XC indicated that GCaMP3-XO or GCaMP3-XC no longer accumulated in the nucleus in contrast to GCaMP3 (Fig. 5a)





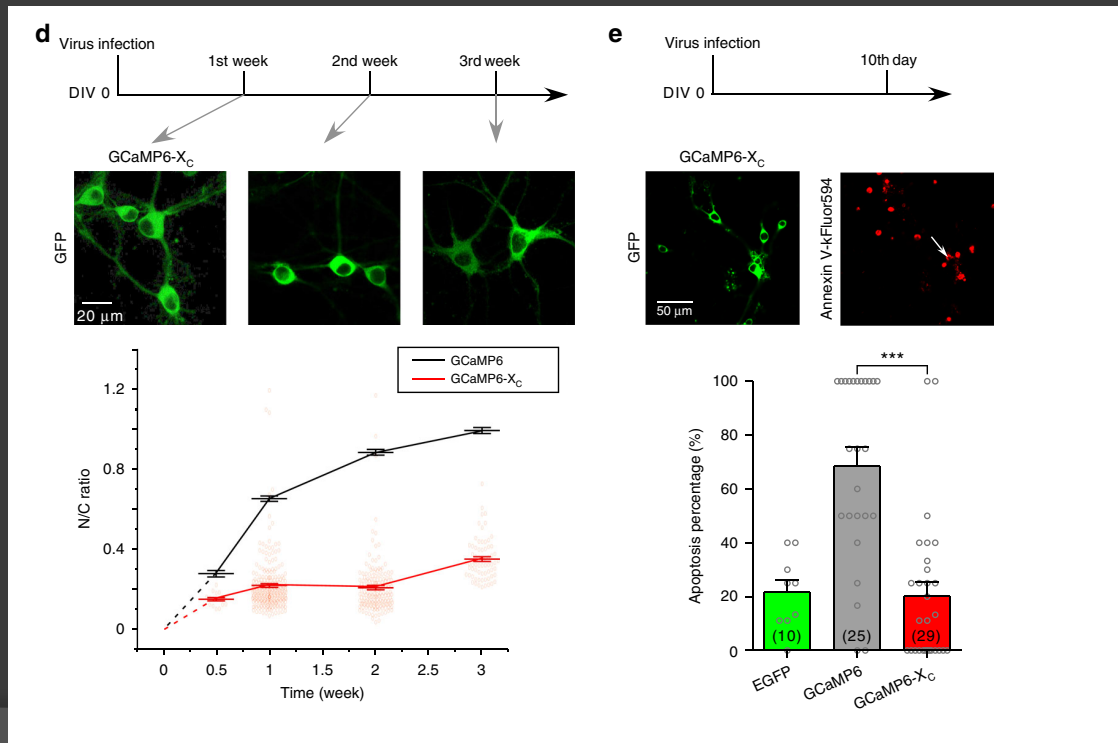
# GCaMP-X no longer perturbs CaV1 signaling in neurons.

Consistent with the profiles of N/C ratios, no more perturbation on pCREB signals (Fig. 5b) and neurite outgrowth (Fig. 5c) could be observed when GCaMP-XO or GCaMP-XC were overexpressed in cortical neurons.



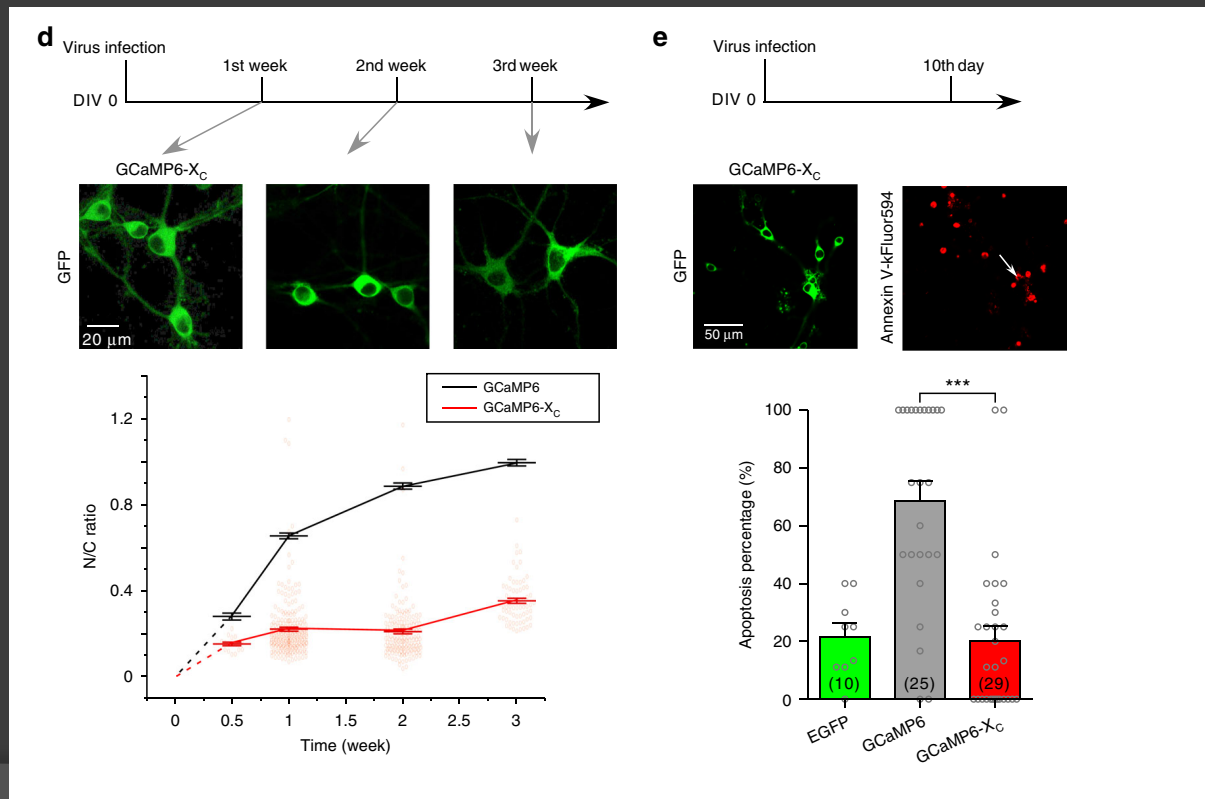
# GCaMP-X no longer perturbs CaV1 signaling in neurons.

Furthermore, we examined the neurons infected with AAV- Syn-GCaMP6m-XC vs. conventional GCaMP. Different from AAV-Syn-GCaMP6f, long-term infection of AAV-Syn-GCaMP6m-XC no longer caused the time-dependent nuclear accumulation in neurons; instead, rather stable cytosolic distributions were maintained: N/C ratio was  $0.36 \pm 0.01$  ( $n = 69$ ) even after three weeks (Fig. 5d).



# GCaMP-X no longer perturbs CaV1 signaling in neurons.

And for apoptosis associated with GCaMP, neurons of 10 days after virus infection of AAV- Syn-GCaMP6m-XC exhibited much weaker apoptotic signals of fluorescent Annexin V (<20% neurons), almost back to the level of control neurons (Fig. 5e)

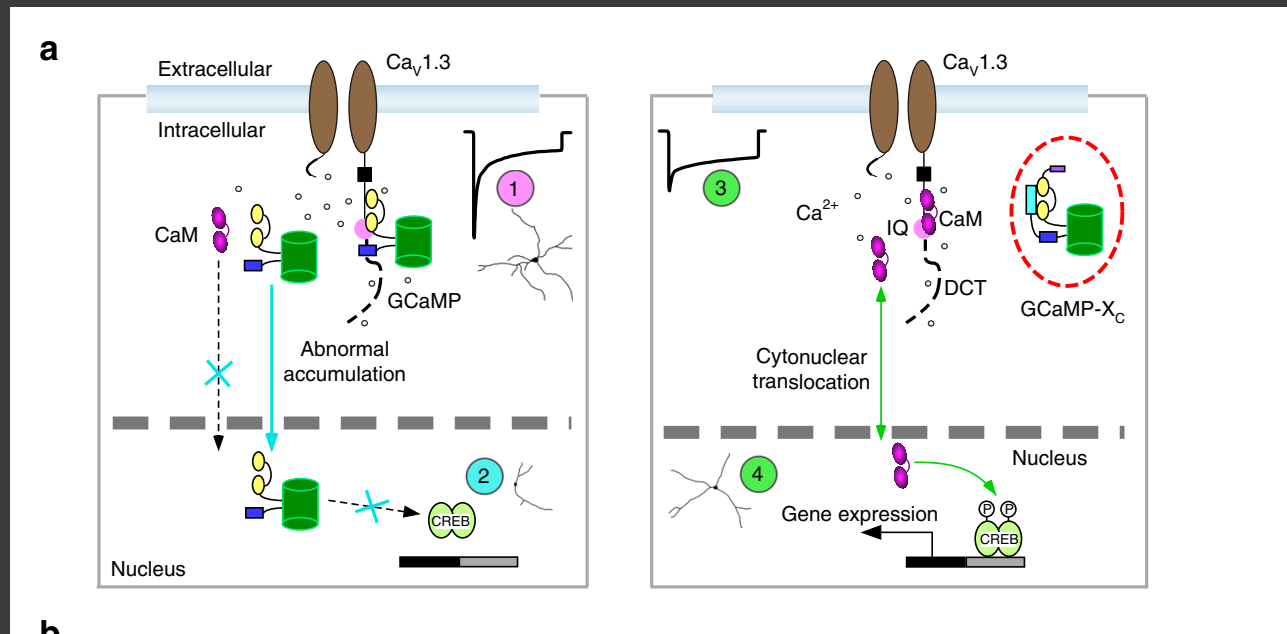


# GCaMP-X no longer perturbs CaV1 signaling in neurons.

To this end, all the known side-effects related to CaV1-dependent transcriptional signaling were all eliminated or strongly attenuated by our newly designed GCaMP-X.

# GCaMP-X no longer perturbs CaV1 signaling in neurons.

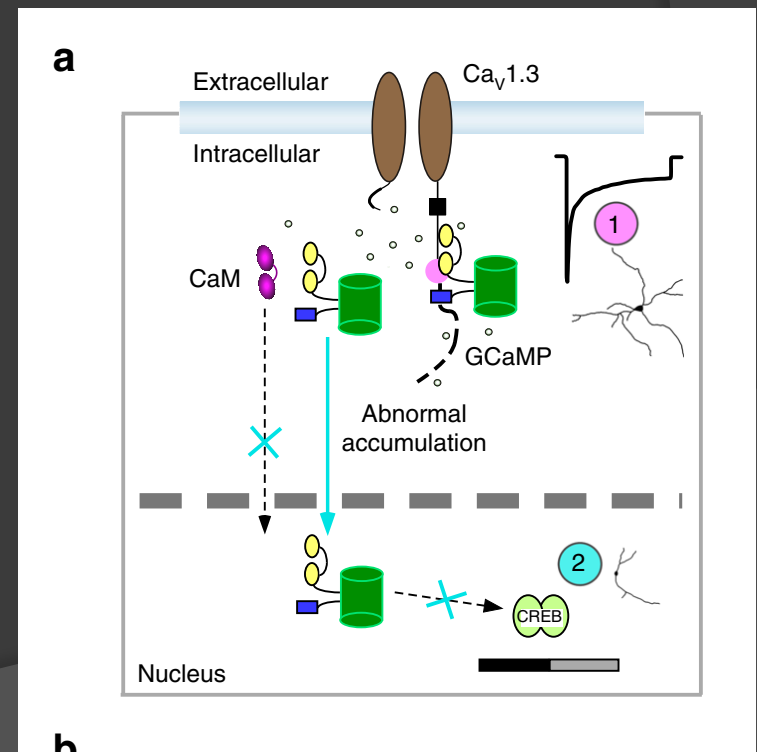
As summarized in the scheme (Fig. 6a), GCaMP defects and mechanisms are clarified by this work, as the basis for the new design of GCaMP-X.



# GCaMP-X no longer perturbs CaV1 signaling in neurons.

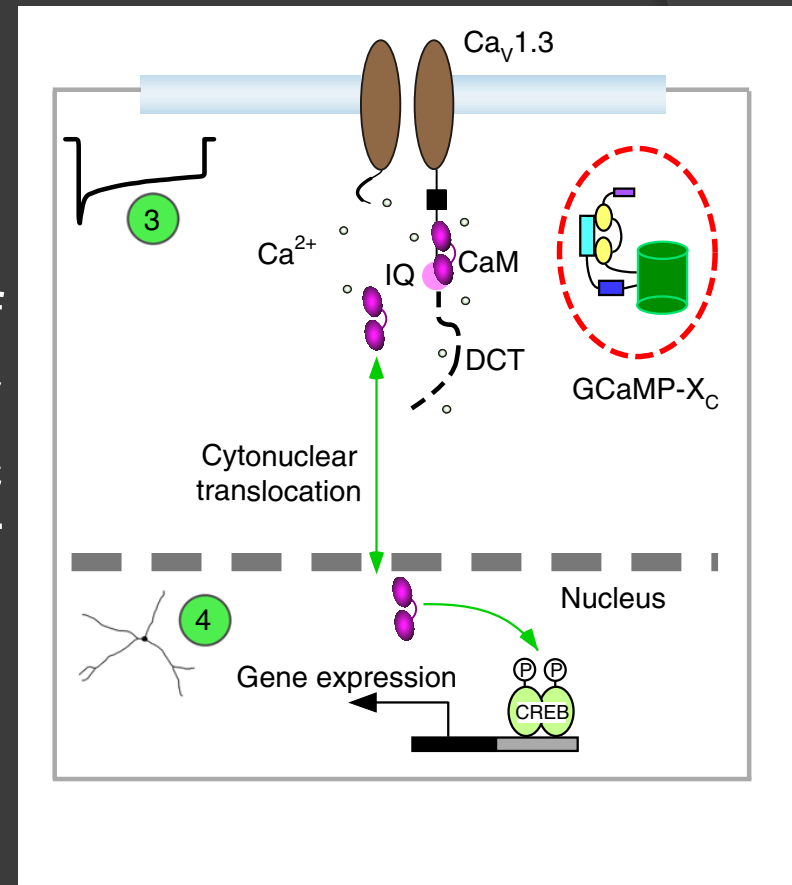
In neurons, GCaMP sensors behave as CaM-like proteins. In consequence, CaV1 gating is perturbed through apoCaM and subsequent Ca<sup>2+</sup>/CaM modulation, causing unexpected increase of Ca<sup>2+</sup> influx and distorted channel kinetics, accumulated nuclear GCaMP, impaired cytonuclear CaM translocation, aberrant gene transcription, and dysregulated growth of neurites.

The general health of neurons is impaired and overall Ca<sup>2+</sup> dynamics is altered, both of which would affect sensor readouts.



# GCaMP-X no longer perturbs CaV1 signaling in neurons.

In contrast, the GCaMP-X sensors containing extra protective motif of apoCaM-binding CBM successfully avoid all the above problematic effects on CaV1-dependent E-T coupling..



# Sensor performance of GCaMP-XC is comparable to GCaMP.

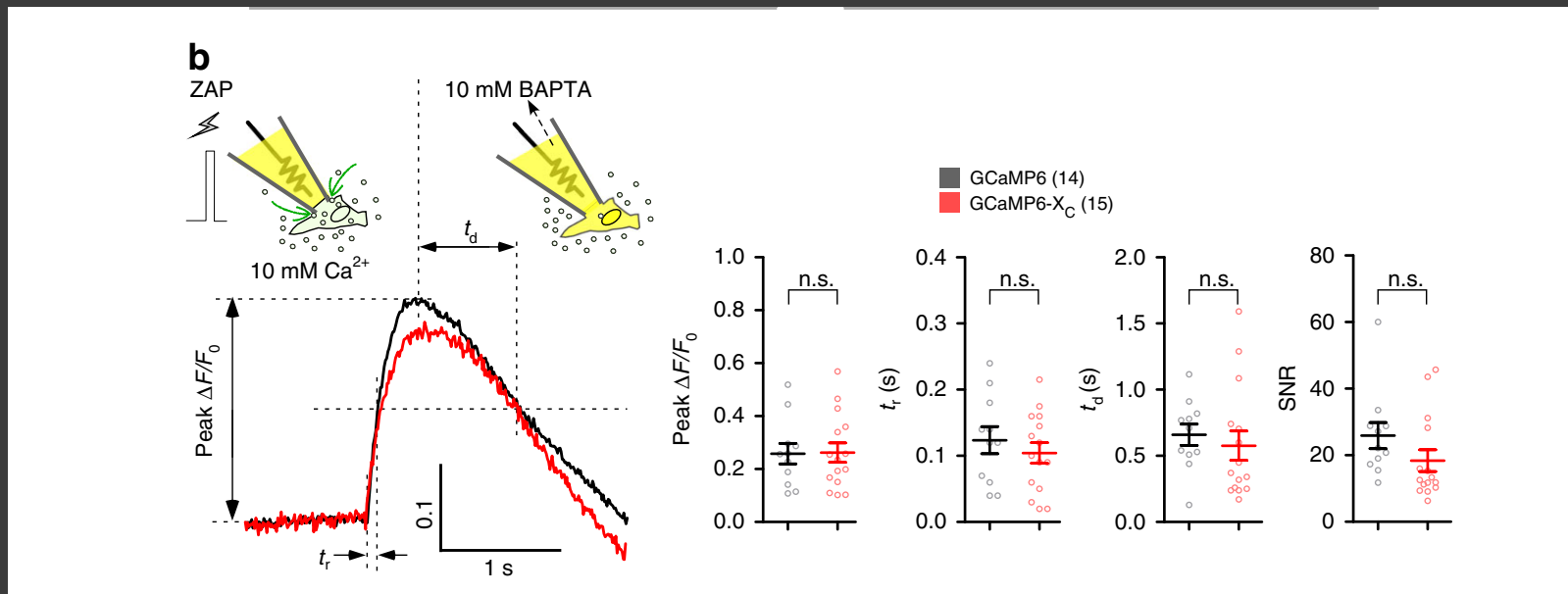
GCaMP-X does not introduce any de novo mutations on the part of GCaMP and CBM would not interfere with  $\text{Ca}^{2+}$ /CaM binding of M13 within GCaMP, thus unlikely to affect its performance as  $\text{Ca}^{2+}$  sensors.

HEK293 cells in response to 10  $\mu\text{M}$  acetylcholine (Ach) were used as the cellular context to fairly compare basic sensor characteristics such as  $\text{Ca}^{2+}$  sensitivities, which turned out to be indistinguishable between GCaMP and GCaMP-XC



# Sensor performance of GCaMP-XC is comparable to GCaMP.

GCaMP6m and GCaMP6m-XC resulted into indistinguishable characteristics of peak  $\Delta F/F_0$ , SNR, rise time  $t_r$  and decay time  $t_d$  (Fig. 6b).



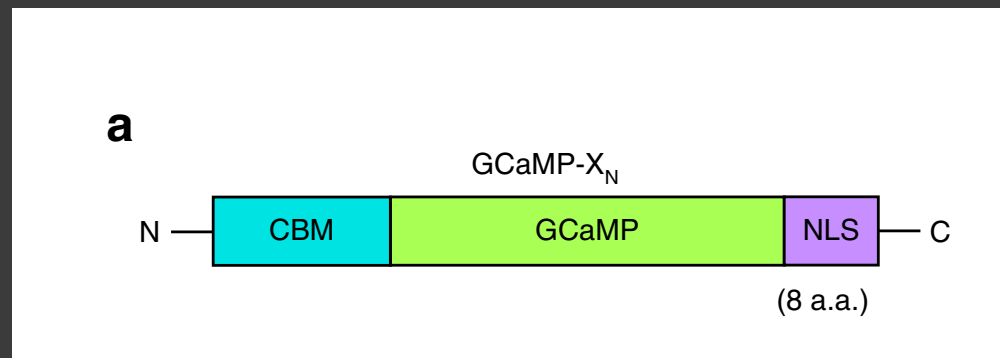
# GCaMP-X as a novel type of nuclear $\text{Ca}^{2+}$ sensors.

In neurons, nuclear  $\text{Ca}^{2+}$  could act as the controlling factor over transcription signaling and gene expression.

Organic fluorescent dyes such as Fura-2 may help explore  $\text{Ca}^{2+}$  dynamics in the nuclear.

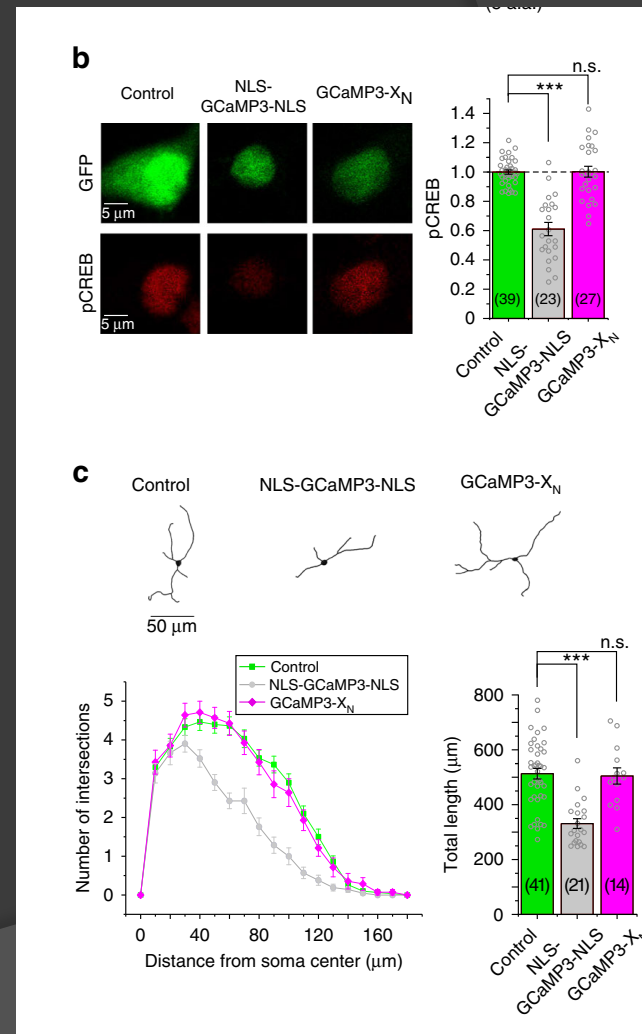
# GCaMP-X as a novel type of nuclear Ca<sup>2+</sup> sensors.

Greatly encouraged by GCaMP-X prototypes which successfully eliminate deleterious side-effects, we proceeded to design a new type of GCaMP-XN targeting genuine and intact nuclear Ca<sup>2+</sup> without aforementioned perturbations. GCaMP-XN is based on GCaMP-X but with NLS (nuclear localization signal) motif fused onto the C-terminus.



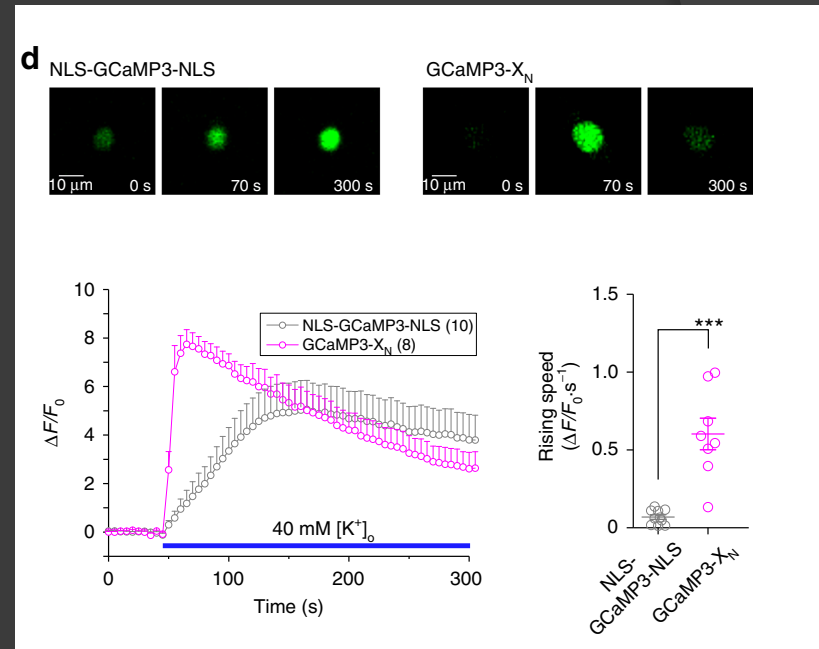
# GCaMP-X as a novel type of nuclear Ca<sup>2+</sup> sensors.

We validated GCaMP-XN by examining and comparing pCREB signals and neurite outgrowth in cortical neurons transfected with NLS-GCaMP3-NLS vs. GCaMP3-XN. Neurons expressing GCaMP3-XN exhibited similar levels of pCREB and neurite outgrowth as the control neurons, whereas NLS-GCaMP3-NLS exhibited strong pCREB inhibition and caused neurite damages (Fig. 7b, c), demonstrating the advantages of GCaMP-XN over conventional GCaMP as sensors of nuclear Ca<sup>2+</sup>.



# GCaMP-X as a novel type of nuclear $\text{Ca}^{2+}$ sensors.

In cortical neurons stimulated by 40mM  $[\text{K}^+]_o$ , GCaMP3-XN with confocal fluorescence imaging resulted into more pronounced (larger peak of  $\Delta F/F_0$ ) and faster (8-fold rising speed in  $\Delta F/F_0 \cdot \text{s}^{-1}$ )  $\text{Ca}^{2+}$  dynamics than NLS-GCaMP3-NLS (Fig. 7d).



# Conclusions

In this work, we conducted in-depth **analyses on the mechanisms of the “side-effects”** existing to widely-applied **GCaMP sensors** in  $\text{Ca}^{2+}$  fluorescence imaging.

Data unveiled that **GCaMP interferes with  $\text{CaV1}/\text{CaM}$ -mediated excitation–transcription coupling in neurons.**

With these novel insights, we then **developed new GCaMP-X** sensors immune to side-effects for faithful monitoring of  $\text{Ca}^{2+}$  dynamics in cells including specific subcellular compartments, e.g., cytosol (GCaMP-XC) or nucleus (GCaMP-XN) or plasma membrane (GCaMP-XM).

The key is to **supply GCaMP** with an **extra motif of high-affinity apoCaM-binding**, which eliminates GCaMP perturbations on apoCaM and its subsequent  $\text{Ca}^{2+}/\text{CaM}$  signaling endogenous to the native cell or particularly its  $\text{CaV1}$  channels.

This way, GCaMP-X sensors resolved all the problems of GCaMP, while still inheriting its excellent sensing capabilities in monitoring  $\text{Ca}^{2+}$  dynamics.